# PSVM: A global database for the Miocene indicating elevated paleosecular variation relative to the last 10 Myrs.

Yael Annemiek Engbers[1], Richard K. Bono[1], and Andrew Biggin[1]

[1]University of Liverpool

November 26, 2022

**Abstract**

Statistical studies of paleosecular variation (PSV) are used to infer the structure and behavior of the geomagnetic field. This study presents a new database, PSVM, of high-quality directional data from the Miocene era (5.3 – 23 Ma), compiled from 1,454 sites from 44 different localities. This database is used to model the latitude dependence of paleosecular variation with varying selection criteria using a quadratic form after Model G. Our fitted model parameter for latitude-invariant PSV (Model G a) is 15.7° and the latitude dependent PSV term (Model G b) is 0.23. The latitude invariant term is substantially higher than previously observed for the past 10 Myrs or any other studied era. We also present a new stochastic model of the time-average field, BB-M22, using a covariant giant Gaussian process (GGP) which is constrained using data from PSVM and Earth-like geodynamo numerical simulations. BB-M22 improves the fit to PSVM data relative to prior GGP models, as it reproduces the higher VGP dispersion observed during the Miocene. Our findings suggest a more variable magnetic field and more active geodynamo in the Miocene era than the past 10 Myrs, perhaps linked to stronger driving by elevated core-mantle heat flow. Although our results support that the average axial dipole dominance of the time-instantaneous field was lower than in more recent times, we note that based on inclination anomaly estimates cannot rule out that the Miocene time averaged field resembles a geocentric axial dipole.

# PSVM: A global database for the Miocene indicating elevated paleosecular variation relative to the last 10 Myrs.

Y. A. Engbers[1], R. K. Bono[1,2] and A. J. Biggin[1]

[1] Geomagnetism Laboratory, Department of Earth, Ocean and Ecological Sciences, University of Liverpool, Liverpool L69 7ZE, United Kingdom

[2] Department of Earth, Ocean and Atmospheric Science, Florida State University, Tallahassee, Florida 32306, United States

**Key Points**

- We compiled a new database, PSVM comprising 1,454 paleomagnetic directions from 44 different localities of Miocene volcanics
- Virtual geomagnetic pole dispersions indicate a more variable field during the Miocene compared to the last 10 Myrs
- The elevated equatorial virtual geomagnetic pole dispersion may imply more vigorous convection in the outer core during this time

**Abstract**

Statistical studies of paleosecular variation (PSV) are used to infer the structure and behavior of the geomagnetic field. This study presents a new database, PSVM, of high-quality directional data from the Miocene era (5.3 – 23 Ma), compiled from 1,454 sites from 44 different localities. This database is used to model the latitude dependence of paleosecular variation with varying selection criteria using a quadratic form after Model G. Our fitted model parameter for latitude-invariant PSV (Model G a) is 15.7° and the latitude dependent PSV term (Model G b) is 0.23. The latitude invariant term is substantially higher than previously observed for the past 10 Myrs or any other studied era. We also present a new stochastic model of the time-average field, BB-M22, using a covariant giant Gaussian process (GGP) which is constrained using data from PSVM and Earth-like geodynamo numerical simulations. BB-M22 improves the fit to PSVM data relative to prior GGP models, as it reproduces the higher VGP dispersion observed during the Miocene. Our findings suggest a more variable magnetic field and more active geodynamo in the Miocene era than the past 10 Myrs, perhaps linked to stronger driving by elevated core-mantle heat flow. Although our results support that the average axial dipole dominance of the time-instantaneous field was lower than in more recent times, we note that based on inclination anomaly estimates cannot rule out that the Miocene time averaged field resembles a geocentric axial dipole.

**Plain Language Summary**

The variability of the magnetic field is dependent on characteristics of the geodynamo in the Earth's outer core. Changes of the geomagnetic field throughout Earth's history are important to study as they give us insight into the evolution of the interior of our planet. We study the changes of the magnetic field using data from volcanic rocks that preserved the magnetic field direction from when they were formed. In this study we gathered all the data from the Miocene period (23 – 5 million years ago) to see how the geomagnetic field was behaving during that time. The database shows that the magnetic field in the Miocene was more variable than in the past 10 million years. Studies that have produced simulations of the geodynamo suggest that when the outer core undergoes stronger convection, this produces a more variable and complicated geomagnetic field at the surface. The higher variability of the geomagnetic field in the Miocene therefore suggests more vigorous convection in the outer core at that time.

## 1. Introduction

Earth's magnetic field is generated by convecting iron in the liquid outer core, a system referred to as the geodynamo. Using paleomagnetic records and geomagnetic observations, knowledge on the changes of the structure and strength of the magnetic field through time can be acquired. These changes of the magnetic field on $10^2 - 10^6$ year timescales are referred to as paleosecular variation (PSV). PSV is often used to study the field structure over timescales of several millions of years or longer (Johnson & McFadden, 2007). Multiple PSV studies investigating the last 5 myr (million years) have been carried out (Johnson et al., 2008; Johnson & Constable, 1996; McElhinny & McFadden, 1997). Cromwell et al. (2018) provided a database of the paleomagnetic directional data for 0 – 10 Ma (PSV10) for the purpose of studying PSV. Compilations of PSV data for older intervals have been published, including the Cretaceous and Jurassic (Doubrovine et al., 2019) and the Precambrian (Smirnov et al., 2011; Veikkolainen & Pesonen, 2014). Comparing the PSV behavior of the field in these different time periods allows for insight in the variability and evolution of the geodynamo.

In this study we present a compilation of published high-quality paleomagnetic directional data for the Miocene (5.3 – 23 Ma). We focus on rapidly cooled volcanic rocks, as they provide an instantaneous record of Earth's magnetic field. We compiled 1454 paleomagnetic directions from lava flows in the Miocene. With this new database, from here on referred to as PSVM (paleosecular variation of the Miocene), we aim to provide insight into the behavior of the magnetic field in the Miocene using statistical PSV models.

The latitudinal dependence of dispersion of virtual geomagnetic pole (VGP) positions is a useful tool to study PSV in a statistical manner. Model G (Mcfadden et al., 1988) is a commonly used description of the magnetic field variability versus latitude. This specific relationship between latitude and VGP dispersion was described by the functional form: $S_b(\lambda) = \sqrt{a^2 + (b\lambda)^2}$, where $S_b$ is the VGP dispersion, $\lambda$ is latitude and $a$ and $b$ represent the VGP dispersion at the equator and the latitudinal dependence of $S_b$, respectively. This relationship has previously been used to describe a similar timeframe as the Miocene. McFadden et al. (1991) created a Model G trend for the 5 – 22.5 Ma, based on 5 datapoints, which is arguably insufficient to robustly describe the variability of the geomagnetic field.

Another method of modelling the statistical variations of the paleomagnetic field are Giant Gaussian Process (GGP) models. These are originally described by CP88 (Constable & Parker, 1988) for the last 5 Myr, with alternative models including QC96 (Constable & Johnson, 1999; Quidelleur & Courtillot, 1996; Tauxe & Kent, 2004). More recently, renewed versions of these GGP family models, BB18 (Bono

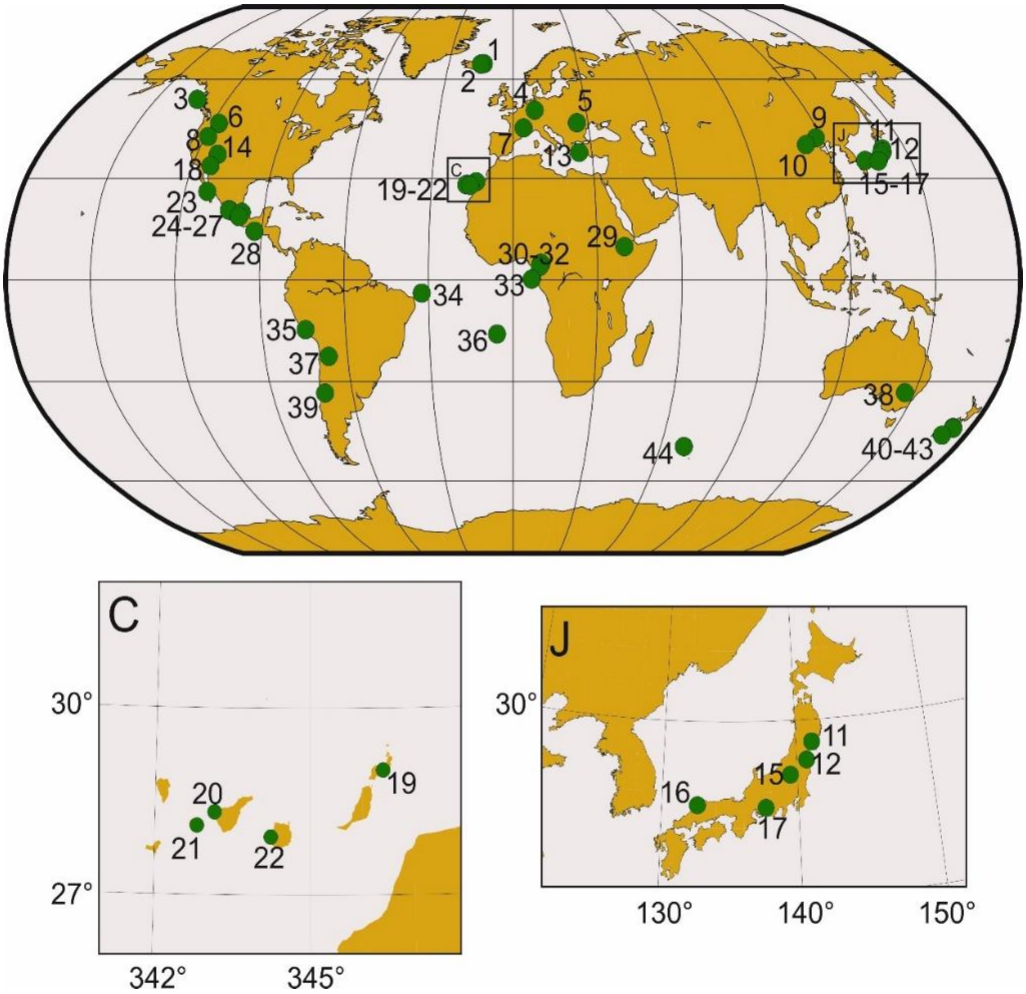


*Figure 1; PSVM locality locations. Numbers correspond to the groups listed in Table 1. Boxes C and J are enlargements of the Canary Islands and Japan, respectively.*

et al., 2020) and BCE19 (Brandt et al., 2020) were presented. These GGP models describe PSV through a description of statistical variability in the Gauss coefficients. They assume most of the non-dipole terms have a zero mean and standard deviation which varies as a function of degree *l* using a scaling term α. The only coefficients that do not have a zero mean are the axial dipolar term $g_1^0$ and, in some models, the quadrupole term $g_2^0$ (e.g., CP88; Constable & Parker, 1988). BB18.Z3 (Bono et al., 2020) also introduced a mean octupole $g_3^0$ term in addition to the non-zero mean $g_2^0$ term. TK03 added an additional scaling term, β, for the specific Gauss coefficients for which *l* - *m* is odd (describing the equatorially asymmetric field), as well as setting the quadrupole term to 0 resulting in a geocentric axial dipole (GAD) only model. GGP models are statistical descriptions of the magnetic field that assume the Gauss coefficients $g_l^m$ and $h_l^m$ are normally distributed. Except for BB18, GGP models also assume that Gauss coefficient distributions are independent. In Bono et al. (2020), a new family of the GGP style models, BB18, was presented where a covariance was defined between certain Gauss coefficients ($l \leq 4$) based on a wide range of “Earth-like” dynamo simulations. BB18 is created by incorporating that covariance between certain Gauss coefficients and with $g_1^0$, and α and β based on paleointensity and PSV data from the PINT database (Biggin et al., 2015; Biggin et al., 2009) for the past 10 Myrs and PSV10 (Cromwell et al., 2018), respectively. Combining the covariance observations derived from dynamo simulations with PSV and V(A)DM data from other intervals it is possible to create new covariant GGP models within the same BB18-style family. In this study, the PSVM and the PINT databases were used to create a new BB18-style model that describes the magnetic field in the Miocene.

Comparisons will be made between our data from PSVM and PSV for the last 10 Myrs (PSV10; (Cromwell et al., 2018)). Additionally, new Model G and BB18 like descriptions specified for the Miocene are presented and compared to those existing for the last 10 Myrs. The new Model G predictions will also be used to relate the magnetic field in the Miocene to studies from other eras such as the Permian-Carboniferous Reverse Super Chron (PCRS) (Handford et al., 2021; de Oliveira et al., 2018), the Post-PCRS (Handford et al., 2021) and the Jurassic and the Cretaceous Normal Super Chron (CNS) (Biggin et al., 2008; Doubrovine et al., 2019). For the last 10 million years both PSV10 (Cromwell et al., 2018) as the updated version of PSV10 (here after referred to as PSV10a) by de Oliveira et al. (2021) will be used.

## 2. The PSVM compilation

### 2.1. General selection criteria

PSVM is a compilation of published studies that report directional data from volcanic sites. We used multiple online resources to find as many Miocene directional studies as possible. These included the online MagIC Database *(http://earthref.org/MAGIC)*, online search engines like Scopus, Google Scholar and the global paleomagnetic database GPMDB *(http://www.iggl.no/resources.html)*. In total 1454 sites were included, all of which met the following criteria:

1. The age of the rock was constrained to a precision that was sufficient to demonstrate that they formed within the Miocene.
2. Principle component analyses (PCA) (Kirschvink, 1980) was used to determine the ChRM component, ensuring that the characteristic direction is isolated. Sites where the characteristic component was suspected to have been affected by remagnetization were excluded.
3. The sites studied were free from significant deformation unless a structural correction could be applied based on field observations (i.e. restored to paleohorizontal). Sites that showed evidence for post-emplacement tilt or other deformation that could not structurally be corrected were left out of the database.

(a) Sites that showed post emplacement block rotation that was the same for the entire locality were still included in the study as this does not affect PSV, but they were excluded from the inclination anomaly analyses as the mean direction cannot be trusted. This was the case for 6 localities.

4. Studies included were not aimed at transitions or excursions. Transitional results are acceptable, however it had to be clear that the entire study area was sampled, and not just the flows that captured the transition or excursion.
5. Sufficient time was sampled such that secular variation was likely to have been averaged sufficiently in the included studies. As typical for paleomagnetic study, we consider a site to be a singular cooling unit that records a geologically instantaneous snapshot of the magnetic field. At least 10 sites (N≥10) per locality were required for inclusion in our dataset. If the authors of the original study commented on a rapid eruption rate or other reason to believe secular variation was not sufficiently sampled, those studies were excluded. We imposed a further constraint to ensure time-averaging: the paleomagnetic direction for each site within a locality must be determined from at least 3 samples ($n \geq 3$) with a precision parameter, k, of 30 or higher.

Together, the requirements defined above are named Selection Criteria Set 1 (CS1) and were the minimum requirements for inclusion in PSVM. Additional selection criteria were implemented for various further analyses of PSVM and these are discussed in section 3.

## 2.2. General statistics of PSVM

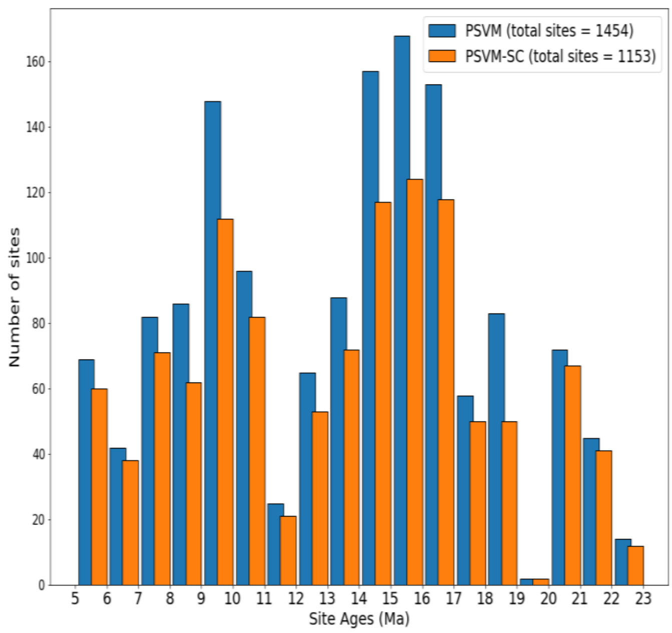


*Figure 2; Age distribution of all PSVM sites (blue) and all PSVM-SC (serial correlation correction) sites (orange) in 1 myr intervals.*

| Locality | Study | Lat | Long | Mlat | Mlong | Age | *N* | *N*-SC | 2R | ΔI | Location | Reference |
|---|---|---|---|---|---|---|---|---|---|---|---|---|
| 1 | 1 | 65.157 | 346.344 | 63.320 | 344.100 | 12 - 13 | 65 | 49 | Y | Y | Iceland | Linder & Leonhardt (2009) |
| 2 | 2 | 65.012 | 344.988 | 64.118 | 343.932 | 5.3 – 7.0 | 22 | 20 | Y | Y | Iceland | Døssing et al. (2020) |
| 3 | 3 | 53.700 | 227.300 | 57.125 | 231.858 | 21.5 | 13 | 11 | N | N | Canada | Irving et al. (2000) |
| 4 | 4 | 50.375 | 8.895 | 48.157 | 5.005 | 16.5 | 34 | 28 | Y | Y | Germany | Sherwood (1990) |
| 5 | 5 | 46.526 | 25.553 | 45.912 | 24.045 | 5.6 | 28 | 23 | N | Y | Romania | Vişan et al. (2016) |
| 6 | 6 | 46.371 | 242.609 | 47.977 | 245.287 | 6.2 - 15.6 | 92 | 63 | Y | Y | USA | Dominguez & Van der Voo (2014) |
| 7 | 7 | 44.991 | 4.175 | 43.686 | 2.129 | 7.9 - 13.6 | 13 | 13 | N | Y | France | Riisager et al. (2000) |
| 8 | 8 | 42.418 | 241.150 | 44.508 | 244.076 | 16.7 – 18.0 | 82 | 61 | Y | N | USA | Jarboe et al. (2008) |
| 9 | 9 | 42.019 | 117.793 | 43.189 | 114.552 | 6.5 - 22.9 | 25 | 20 | Y | Y | China | Zheng et al. (2002) |
| 10 | 10 | 40.000 | 112.800 | 41.588 | 107.945 | 18 | 30 | 17 | Y | Y | China | Pan et al. (2005) |
| 11 | 11 | 38.752 | 141.211 | 40.934 | 138.158 | 14 | 10 | 10 | N | Y | Japan | Hoshi & Teranishi (2007) |
| 12 | 12 | 37.754 | 140.750 | 40.226 | 137.289 | 16 | 11 | 10 | N | Y | Japan | Takahashi et al. (1999) |
| 13 | 13 | 37.700 | 25.200 | 36.378 | 22.362 | 11.3 - 15.5 | 11 | *< 10* | N | N | Greece | Avigad et al. (1998) |
| 14 | 14 | 37.138 | 247.867 | 38.232 | 248.309 | 5.7 - 9.9 | 20 | 19 | Y | Y | USA | Mankinen (2008) |
| 15 | 15 | 36.953 | 139.481 | 38.481 | 137.346 | 5.5 - 15.5 | 29 | 26 | Y | Y | Japan | Otofuji et al. (1997) |
| 16 | 16 | 35.282 | 132.603 | 37.025 | 128.719 | 10.8 - 16.2 | 14 | 14 | Y | Y | Japan | Otofuji et al. (1991) |
| 17 | 17 | 35.135 | 137.609 | 37.152 | 133.228 | 15.0 - 15.5 | 35 | 34 | Y | Y | Japan | Hoshi & Yokoyama (2001) |
| 17 | 18 | - | - | - | - | - | - | - | - | - | - | Hoshi & Sano (2013) |
| 18 | 19 | 33.792 | 246.681 | 35.552 | 248.927 | 8.5 - 20.1 | 164 | 106 | Y | Y | USA | Calderone et al. (1990) |
| 19 | 20 | 29.000 | 346.400 | 27.534 | 344.949 | 6.0 - 14.5 | 30 | 26 | Y | Y | Lanzarote | Carracedo & Soler (1995) |
| 20 | 21 | 28.325 | 343.145 | 27.457 | 342.261 | 5.7 | 26 | 23 | Y | Y | Tenerife | Leonhardt & Soffel (2006) |
| 21 | 22 | 28.109 | 342.809 | 26.637 | 341.338 | 9.7 - 9.8 | 54 | 30 | N | Y | La Gomera | Glen et al. (2003) |
| 21 | 23 | - | - | - | - | - | - | - | - | - | - | Caccavari et al. (2015) |
| 22 | 24 | 27.930 | 344.231 | 25.760 | 342.029 | 14.1 - 14.3 | 93 | 67 | N | Y | Gran Canaria | Leonhardt & Soffel (2002) |
| 22 | 25 | - | - | - | - | - | - | - | - | - | - | Leonhardt et al. (2000) |
| 23 | 26 | 26.099 | 248.220 | 27.546 | 249.691 | 6.0 - 23.2 | 41 | 39 | Y | Y | Mexico | Hagstrum et al. (1987) |
| 24 | 27 | 20.762 | 257.319 | 21.486 | 258.166 | 7.8 - 10.2 | 13 | 13 | Y | Y | Mexico | Ruiz-Martínez et al., (2010) |

*Table 1 is continued on next page*

| Locality | Study | Lat | Long | Mlat | Mlong | Age | *N* | *N*-SC | 2R | ΔI | Location | Reference |
|---|---|---|---|---|---|---|---|---|---|---|---|---|
| 25 | 28 | 20.605 | 257.265 | 21.430 | 258.259 | 5.9 - 13.0 | 44 | 33 | Y | Y | Mexico | Goguitchaichvili et al. (2011) |
| 26 | 29 | 20.024 | 262.071 | 20.538 | 262.849 | 6.5 - 14.0 | 10 | 10 | Y | Y | Mexico | Ruiz-Martínez et al. (2000) |
| 27 | 30 | 18.680 | 261.252 | 19.961 | 263.071 | 20.7 | 22 | 22 | Y | Y | Mexico | Duarte et al. (2015) |
| 28 | 31 | 14.380 | 267.389 | 13.636 | 264.640 | 15.5 | 34 | 24 | Y | Y | Honduras | Garza et al. (2012) |
| 29 | 32 | 9.873 | 39.745 | 7.431 | 36.823 | 13 | 36 | 35 | Y | Y | Ethiopia | Lhuillier & Gilder (2019) |
| 30 | 33 | 4.909 | 9.864 | 0.903 | 5.370 | 20.1 – 23.0 | 22 | 19 | Y | Y | Cameroon | Ubangoh et al. (1998) |
| 31 | 33 | 4.886 | 10.091 | 1.944 | 6.803 | 14.8 - 16.1 | 22 | 20 | Y | Y | Cameroon | Ubangoh et al. (1998) |
| 32 | 33 | 4.000 | 9.500 | 2.270 | 7.563 | 6.5 - 11.4 | 10 | 10 | Y | Y | Cameroon | Ubangoh et al. (1998) |
| 33 | 34 | 0.294 | 6.620 | -1.024 | 5.106 | 7 | 38 | 33 | Y | Y | São Tomé | Opdyke et al. (2015) |
| 34 | 35 | -3.857 | 327.586 | -4.844 | 327.969 | 9.4 - 10.8 | 13 | 11 | Y | Y | Fernando de Noronha | Leonhardt et al. (2003) |
| 35 | 36 | -14.600 | 285.700 | -15.851 | 286.117 | 20 | 21 | 21 | Y | Y | Peru | Roperch et al. (2011) |
| 36 | 37 | -15.932 | 354.295 | -17.553 | 351.996 | 8.8 - 10.3 | 41 | 35 | Y | Y | Saint Helena | Engbers et al. (2020) |
| 37 | 38 | -22.500 | 293.100 | -23.143 | 293.191 | 9 | 13 | 10 | N | Y | Argentina | Somoza et al., (1996) |
| 38 | 39 | -33.240 | 146.494 | -41.125 | 142.637 | 16 | 13 | *< 10* | N | Y | Australia | Hansma & Tohver (2018) |
| 39 | 40 | -33.359 | 289.723 | -34.545 | 289.560 | 17.6 | 29 | 27 | N | N | Chile | Goguitchaichvili et al. (2000) |
| 40 | 41 | -43.600 | 172.750 | -46.259 | 177.404 | 10.6 | 23 | 19 | Y | Y | New Zealand | Sherwood (1988) |
| 41 | 41 | -43.600 | 172.800 | -45.467 | 176.083 | 7.5 | 14 | 11 | N | N | New Zealand | Sherwood (1988) |
| 42 | 41 | -43.800 | 173.000 | -46.003 | 176.856 | 8.8 | 50 | 34 | Y | N | New Zealand | Sherwood (1988) |
| 43 | 41 | -45.848 | 170.637 | -48.799 | 175.648 | 12 | 14 | 12 | Y | Y | New Zealand | Sherwood (1988) |
| 44 | 42 | -49.300 | 69.500 | -49.044 | 67.231 | 21 | 30 | 28 | Y | Y | Kerguelen Islands | Henry & Plessard (1997) |

Table 1; Locality included in the PSVM compilation. ‘Locality’ is the Locality number which corresponds to the numbers in Figure 1. 'Study' is the Study number. Lat (N) and Long (E) are the average latitude and longitude of the group sites. Mlat (N) and Mlong (E) are the average paleolatitude and paleolongitude corrected for plate motion with the NNR-Morvel model (Argus et al., 2011). Age is the average age or age range in Ma for the studies in one locality group, the precision is given as it is reported in the original study. *N* is the number of sites included in the group, *N*-SC is the number of sites in the group after a serial correlation correction has been applied. The 2R column shows if the locality has at least 2 reversals covered in the data. The ΔI column shows if the locality did or did not experience block rotation and is therefore appropriate for the inclination anomaly analysis. Location refers to the country or island that the group is in. Reference is the short name for the study including first (and sometimes second) author and year of publication.

In total, our PSVM dataset contains directional data from 42 different studies (Table 1), all published between 1987 and 2020. Within the compilation there are 2 studies (Sherwood, 1988; Ubangoh et al., 1998) that sampled different localities within the study, that were divided into separate entries in the database. Other studies were so close in proximity (e.g. when they came from the same small island, or are separated by less than 5°) and sometimes even a continuation of the previous fieldwork or study, we combined them as one locality (e.g. Leonhardt & Soffel, 2002; Leonhardt et al., 2000). Our final database comprises 44 distinct localities. The global distribution of the PSVM localities is portrayed in Figure 1. Most of the localities (32/44) in the database are in the northern hemisphere, due to the large number of localities sampling North America. The age distribution of sites tends to decline for ages older than 20 Ma (Figure 2), however, there does not appear to be the strong prioritization of any given interval. The uniformity of site ages is in contrast with the last 10 myr, where the Brunhes chron (0-0.78 Ma) is heavily sampled relative to older time intervals (Cromwell et al., 2018).

### 2.3. Additional selection criteria

Defining selection criteria for a paleomagnetic database, particularly for paleosecular variation, is non-trivial due to the need to balance between data quantity and data quality. Common criteria for directional data are based on defining a minimum number of specimens used to define the site-mean ($n$) and the maximum amount of within-site dispersion permitted (either the precision parameter $k$ or the corresponding 95% confidence ellipsoid about the mean direction, $\alpha_{95}$)(Fisher, 1953). When the number of samples, $n$, is reported, precision parameter $k$ and $\alpha_{95}$ can be related using the following equation:

$$\cos\alpha_{(1-p)} = 1 - \frac{n-R}{R}\left\{\left(\frac{1}{p}\right)^{\frac{1}{n-1}} - 1\right\}, \qquad k = \frac{n-1}{n-R} \qquad (1)$$

Where $p$ is the significance level, typically set to 0.05 to obtain the confidence limit $\alpha_{95,}$ $n$ is the numbers of samples used to calculate the site-mean and $R$ is the resultant vector of the site-mean. A relatively relaxed set of selection criteria (CS1; $k > 30$, $n \geq 3$) was chosen to maximize the amount of data compiled for the Miocene, to allow for future PSVM users to define their own selection criteria. For our PSV analyses, we explored combinations of minimum thresholds ($k > 30$ and $n \geq 3$, $k > 50$ and $n \geq 4$, $k > 50$ and $n \geq 5$, $k > 75$ and $n \geq 5$).

A common concern with PSV studies is ensuring that the minimum number of sites (e.g., $N \geq 10$) for a given locality is sufficient to average secular variation properly. To address this concern, we apply a further criterion to our analyses of requiring that at least 2 reversals were sampled within a locality.

Any locality that did not contain at least two reversals were excluded from the subset of the database called $PSVM^{2R}$. PSVM contains 12 localities with less than 2 reversals, leading to $PSVM^{2R}$ containing 32 localities, when the general selection criteria (CS1) are applied. Localities consisting of a large stack of lava flows may have formed on shorter timescales than required to average secular variation (referred to as serial correlation, SC). Localities where serial correlation is a concern can be handled through the application of a correction, for which the method is described in Supplementary Material Section S1. $PSVM^{SC}$ is the subset of the database when corrected for SC, and $PSVM^{SC\text{-}2R}$ is the subset when corrected for SC after excluding the localities with less than 2 reversals.

In total we have 5 different subsets of the PSVM database (PSVM, $PSVM^{SC}$, $PSVM^{2R}$, $PSVM^{SC\text{-}2R}$, $PSVM^{\Delta I}$). The last version, $PSVM^{\Delta I}$ is the version used for inclination anomaly (ΔI). As we need the true inclination to calculate the inclination anomaly, the six localities that have experienced block rotations that could not be corrected for with plate corrections are excluded, as described in criteria 3a in section 2.1. Different sets of selection criteria (for *k* and *n)* can be applied to each of these subsets, leading to 16 different subsets of the database with different criteria (CS1 – CS16) that we used for our statistical analyses (Supplementary Material Table S1).

## 3. VGP dispersion and Inclination anomaly

Virtual geomagnetic poles (VGPs) and their dispersion were calculated for each locality for each set of selection criteria using the PSVM database. The VGP latitude and longitude for each site were calculated using the provided inclination and declination and a modeled paleolocation. Paleolocations were determined by reconstructing present day site locations to the mean reported age for the sampled cooling units using the NNR-MORVEL56 plate motion model (Argus et al., 2011). For the VGP dispersion, our sites were grouped into the localities as described in section 2. We chose not to calculate the VGP dispersion based on latitude bins as done in some other PSV studies (e.g. Cromwell et al., 2018) to be able to include the studies that experienced coherent block rotation and to be able to compare to older eras for which latitude binning is impossible due to imprecise paleogeographic constraints. The VGP dispersion was calculated based on the equation:

$$S_b = \sqrt{\frac{1}{N-1}\sum_{i=1}^{N}\left(\Delta_i^2 - \frac{S_{w_i}^2}{n_i}\right)} \tag{2}$$

Where $\Delta_i$ represents the angular deviation of *i*th sites VGP to the mean of the VGPs, $N$ is the number of sites, and *n* is the number of samples within the site, $S_w$ is the within site dispersion calculated from *k*. $S_b$ represents the dispersion of the magnetic signal, after correcting for the within-site dispersion $S_w$ determined from *n* samples (Dominguez & Van der Voo, 2014; Johnson et al., 2008). The VGP dispersion was calculated using both the iterative Vandamme cut-off (Vandamme, 1994) and a fixed 45° cut-off for all 16 different subsets.

### 3.1. Model G values *a* and *b* with different selection criteria

The VGP dispersion for each locality is plotted with their paleolatitude (i.e. Figure 3, Supplementary Material Figure S1 and S2). For each subset, different Model G *a* and *b* parameters were calculated by finding the minimum of the squared deviations between $S_b$ for the data and the Model G-style fit. A confidence interval for those *a* and *b* values was estimated through a nonparametric resampling with replacement of the $S_b$ data that were used as input for the Model G calculations (Doubrovine et al., 2019; Sprain et al., 2019). The *a* and *b* values for each of the PSVM selection criteria subsets can be found in Supplementary Material Table S1. Henceforth, we will focus on subsets with the following 7 selection criteria sets (CS 1 – 4, CS7, CS11, CS15) from Supplementary Material Table S1:

CS1: all data in PSVM, $k > 30$, $n \geq 3$
CS2: $k > 50$, $n \geq 4$, same selection criteria as PSV10
CS3: $k > 50$, $n \geq 5$
CS4: $k > 75$, $n \geq 5$
CS7: $k > 50$, $n \geq 5$, at least 2 reversals per locality ($PSVM^{2R}$)
CS11: $k > 50$, $n \geq 5$, corrected for serial correlation ($PSVM^{SC}$)
CS15: $k > 50$, $n \geq 5$, corrected for serial correlation, at least 2 reversals per locality ($PSVM^{SC\text{-}2R}$)

The Model G predictions for these 7 subsets of PSVM are presented in Table 2 and plotted in Supplementary Material Figures S1 and S2, for both Vandamme and 45° cut-off, with their 95% uncertainty bounds. For each Model G prediction, we calculated the root mean square (RMS) misfit and $\chi^2$ between the trend and the datapoints (Table 2). The $\chi^2$ (Eq. 3; Pearson, 1900; Press et al., 1992) represents the cumulative value of the square of the misfits between the expected value ($E_i$, or Model G prediction) and the observed value ($O_i$, $S_b$ from the data) divided by the expected value.

$$\chi^2 = \sum \frac{(O_i - E_i)^2}{E_i} \tag{3}$$

For all the scenarios where a 45° cut-off was applied, the hypothesis that Model G is an appropriate description of the data could not be rejected with 95% confidence. The PSVM database produces some localities with relatively high dispersions, most likely due to a higher variability of the field, causing the variable cut-off angle from Vandamme (1994) to increase and include data that the non-variable 45° cut-off angle will reject. The Vandamme cut-off therefore produces a latitudinal dependence for the VGP dispersion that does not follow the Model G trend as well as the 45° cut-off.

*Table 2; Model G prediction values for the 7 different selection criteria subsets of PSVM with both Vandamme (Vandamme, 1994) and 45° cut-off applied. $N_g$ is the number of localities that the Model G prediction is based on. Values a and b are the Model G parameters and their uncertainties. RMS is the root-mean-square misfit between the $S_b$ data and the model curve. For each Model G prediction and database, $\chi^2$ is the statistic for how well the model fits the data. $\chi^2_{95}$ is the upper 5% critical value for $\chi^2$. Selection criteria marked with bold italics is our preferred dataset.*

| | Vandamme cut-off | | | | | | |
|---|---|---|---|---|---|---|---|
| Subset: | $N_g$ | *a*(°) | *b* | RMS(°) | $\chi^2$ | $\chi^2_{95}$ | |
| CS1 | 44 | 19.1 +3.3/-4.1 | 0.21 +0.15/-0.20 | 7.0 | 108.9 | 59.3 | Rejected |
| CS2 | 31 | 17.4 +3.2/-3.4 | 0.21 +0.14/-0.21 | 6.0 | 59.9 | 43.8 | Rejected |
| CS3 | 30 | 18.0 +3.0/-3.7 | 0.17 +0.15/-0.17 | 6.1 | 58.1 | 42.6 | Rejected |
| CS4 | 28 | 17.7 +3.0/-3.7 | 0.17 +0.17/-0.17 | 6.1 | 61.2 | 43.8 | Rejected |
| ***CS7*** | ***23*** | ***15.7 +3.0/-2.7*** | ***0.23 +0.14/-0.23*** | ***4.6*** | ***27.0*** | ***33.9*** | - |
| CS11 | 28 | 18.0 +4.8/-3.9 | 0.26 +0.18/-0.26 | 6.6 | 59.0 | 40.1 | Rejected |
| CS15 | 20 | 15.2 +4.4/-3.9 | 0.32 +0.17/-0.32 | 5.4 | 26.5 | 30.1 | - |
| | 45° cut-off | | | | | | |
| | $N_g$ | *a*(°) | *b* | RMS(°) | $\chi^2$ | $\chi^2_{95}$ | |
| CS1 | 41 | 16.6 +2.1/-2.1 | 0.25 +0.07/-0.09 | 3.1 | 22.6 | 55.8 | - |
| CS2 | 31 | 15.9 +2.4/-2.4 | 0.27 +0.07/-0.08 | 3.5 | 21.0 | 43.8 | - |
| CS3 | 30 | 16.0 +2.4/-2.2 | 0.27 +0.07/-0.09 | 3.4 | 20.0 | 42.6 | - |
| CS4 | 27 | 15.7 +2.4/-2.1 | 0.27 +0.06/-0.10 | 3.3 | 16.6 | 38.9 | - |
| ***CS7*** | ***24*** | ***15.5 +2.1/-2.2*** | ***0.27 +0.07/-0.09*** | ***3.0*** | ***12.3*** | ***35.2*** | **-** |
| CS11 | 28 | 17.2 +2.7/-2.9 | 0.24 +0.09/-0.16 | 3.5 | 18.7 | 40.1 | - |
| CS15 | 20 | 16.5 +2.8/-2.6 | 0.25 +0.10/-0.14 | 3.0 | 9.0 | 30.1 | - |

*Table 3; Model parameters and misfit statistics of selected GGP models, PSVM database is with subset $CS7_{VD}$. Parameters α, β are the scaling parameters according to Constable and Parker (1988) and Tauxe and Kent (2004). $g_1^0$ is the mean Gauss coefficient of degree 0 and order 1. $\sigma_{g_1^0}$ is the standard deviation of the $g_1^0$ term. α, $g_1^0$ and $\sigma_{g_1^0}$ terms are expressed in μT. $\chi^2_{VGP}$ is the misfit between the VGP dispersion estimations of the specified model and the datapoints in the PSVM database (subset $CS7_{VD}$). $\chi^2_{95}VGP$ is the critical value of $\chi^2_{VGP}$ which, when exceeded, implies a rejection of that model is a good description of the database within the 95% confidence bounds. $\chi^2_{\Delta I}$ is the misfit between the inclination anomaly estimation of the specified model and the datapoints in the PSVM database, and $\chi^2_{95}\Delta I$ is again the critical value to determine if a model can be rejected as a good description of our database within the 95% confidence bounds.*

| Model *(database)* | α | β | $g_1^0$ | $\sigma_{g_1^0}$ | $\chi^2_{VGP}$ | $\chi^2_{95}VGP$ | $\chi^2_{\Delta I}$ | $\chi^2_{95}\Delta I$ |
|---|---|---|---|---|---|---|---|---|
| Model G (*PSVM*) | - | - | - | - | 27.0 | 33.9 | - | - |
| BB-M22 (*PSVM*) | 12.33 | 2.2 | -15.08 | 10.3 | 26.9 | 33.9 | 6.5 | 15.5 |
| BB18 (*PSV10*) | 12.25 | 2.82 | -22.04 | 10.8 | 48.2 | 33.9 | 21.8 | 15.5 |
| TK03 (*PSVRL*) | 7.3 | 3.8 | -18 | - | 67.0 | 33.9 | 17.1 | 15.5 |

Both scenarios are presented in this study, but the Vandamme cut-off is preferred to allow the comparison to other eras where PSV was studied and to avoid rejecting sites that are not transitional but simply outliers due to anomalously large PSV. Applying the Vandamme cut-off, the subsets CS1 – 4 and CS11 can all be rejected as well-described by Model G as the $\chi^2$ value exceeds the critical $\chi^2_{95}$

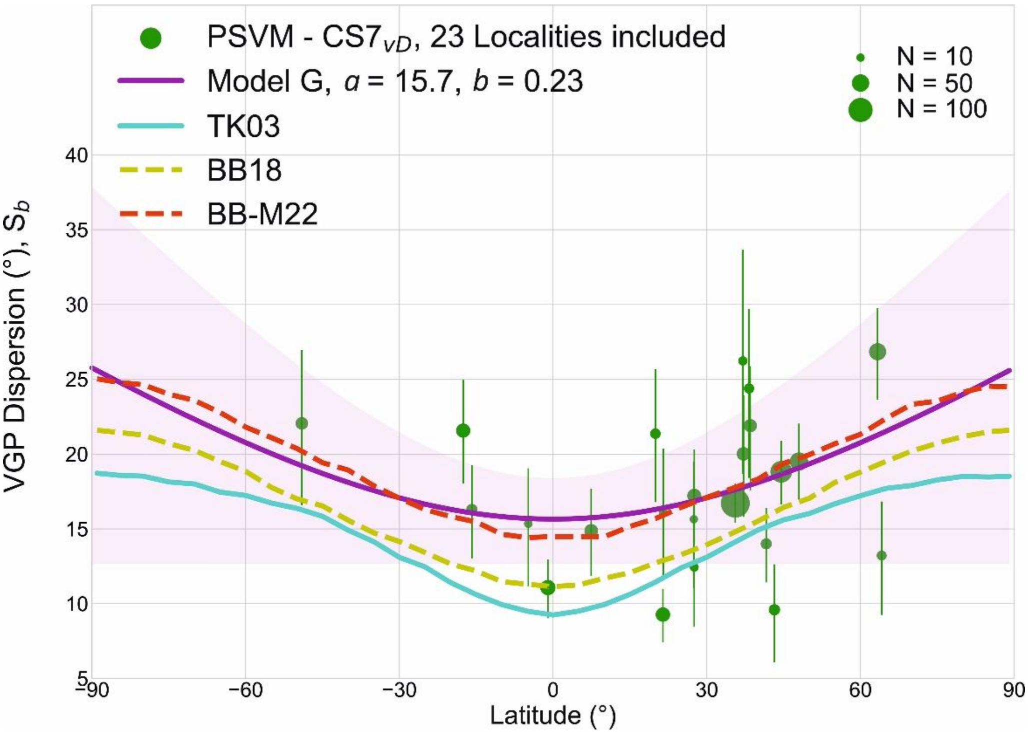


*Figure 3; The VGP dispersion versus latitude for our preferred model for PSVM (CS7$_{vD}$) in green dots (size of dot represents the number of sites in the locality (N)) with the VGP dispersion predictions for Model G (purple line, with pink shaded area as bootstrapped 95% confidence bounds), TK03 (cyan line), BB18 (beige dashed line) and BB-M22 (red dashed line).*

value, which is the upper 5 percent of the $\chi^2$ distribution depending on the degrees of freedom (Table 2; Pearson, 1900). This is apparent from Supplementary Material Figures S1 and S2 and further supports that the criterion of at least 2 reversals is needed to ensure that secular variation is well-represented. The correction for Serial Correlation (SC) as done in CS11 and CS15 runs the risk of overcorrecting, particularly if the field is in a more stable state. As the criterion of 2 reversals already reduces the likelihood that secular variation is not fully captured, we chose CS7 with the Vandamme cut-off (CS7$_{vD}$) as our preferred subset and this is shown in Figure 3. The results for each locality in this preferred subset are presented in Supplementary Material Table S2.

### 3.2. New covariant GGP model, BB-M22, based on PSVM and PINT

A new covariant giant Gaussian process (GGP) model, following (Bono et al., 2020) was created using our preferred subset of PSVM (CS7$_{vD}$). The PINT database (Biggin et al., 2009; Bono et al., 2022) was used to define the paleointensity record from the Miocene needed to determine a mean $g_1^0$ value for this renewed model. The selection criteria *Nint* ≥ 3, $\sigma$ < 5 μT or $\sigma/F$ < 25% and only methods that include pTRM checks, were applied to the Miocene data from the PINT database (Engbers et al. 2022). The parameters α (scaled variance for all Gauss coefficients, defined in Constable & Parker, 1988) and β (additional scalar variance of spherical harmonic l-m odd terms, defined in Tauxe & Kent, 2004) are determined with the use of PSVM divided into 10° latitudinal bins. These values are presented in Table 3, together with the $g_1^0$ , α and β values of BB18 and TK03. The mean $g_1^0$ value was directly determined from the distribution of dipole moment data from PINT, whereas the $\sigma_{g_1^0}$, α and β terms were determined by minimizing the model misfit to VDM variance and VGP dispersion data. In the case of β, due to the high scatter of VGP dispersion estimates, a local minimum in misfit of 2.2 was chosen since this represents some degree of latitude dependence in VGP dispersion. Nevertheless, the absence of a latitude dependence in VGP dispersion cannot be excluded with 95% confidence from our data, resulting in Model G *b* value of 0 and GGP β value of 1 falling within our confidence interval for model values. Our first model, BB-M22, was built on the same concepts as BB18, and applies the same correlation values between certain Gauss coefficients that was observed in Earth-like dynamo simulations (Bono et al., 2020). Figure 3 shows the BB-M22 VGP dispersion curve for PSVM, plus its Model G prediction and the BB18 VGP dispersion curve based on PSV10 (Bono et al., 2020; Cromwell et al., 2018). BB-M22 shows an increased VGP dispersion relative BB18, resulting in a better fit to PSVM observations.

The slightly lower minimum (equatorial) VGP dispersion predicted by BB-M22 seems like a better fit to PSVM than the Model G prediction based on that same dataset. The $\chi^2$ value, as presented in Table 3, to describe the statistical relationship between the PSVM data and BB-M22 (26.9) is indistinguishable from that which describes the relationship between the PSVM data and our Model G prediction curve (27.0). The $\chi^2$ values for the BB-M22 and Model G predictions are lower than the critical $\chi^2_{95}$ value (33.9) suggesting these predictions cannot be rejected as a good description of the data within the 95% confidence bounds. The $\chi^2$ values that describe the fit of the BB18 and TK03 predictions to the PSVM data, exceed the $\chi^2_{95}$ value (48.2 and 67.0, Table 3), and can be rejected as explaining the data at the 95% confidence level.

### 3.3. Inclination Anomaly from PSVM data

Inclination anomaly behavior was studied using the preferred subset of our PSVM database ($CS7_{VD}$). The mean inclination of locality #8 (Steens mountain; Jarboe et al., 2008), was not considered as this study covers a location that experienced local block rotation, which is unsuitable for inclination anomaly analyses (Table 1). Other studies or localities that experienced local block rotations were already excluded due to the strict selection criteria of our preferred subset. The data was split into 10° latitude bins, before calculating the Fisher mean inclination (Fisher, 1953). The mean inclinations were compared to the expected inclination at the specified latitudes as predicted by a GAD field. These predictions follow the equation: $\tan I_{GAD} = 2\ \tan\lambda$, where $\lambda$ is the latitude. The inclination anomaly ($\Delta I$) (Johnson & McFadden, 2015) is the difference between the mean inclination and the predicted GAD inclination at the average paleolatitude of the directional locality within PSVM. In Figure 4, these $\Delta I$ values are compared with the trend in inclination anomaly according to BB18 and BB-M22 and TK03

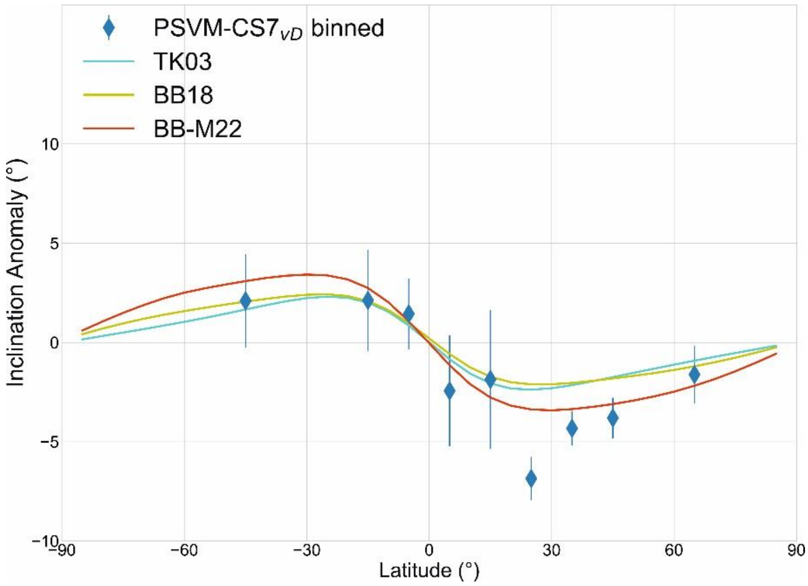


*Figure 4; The inclination anomaly versus latitude for our preferred subset of PSVM (CS7$_{VD}$ excluding locality #8) binned into 10° latitude bins, with the inclination anomaly predictions for TK03 (cyan line), BB18 (beige line) and BB-M22 (red line).*

(Tauxe & Kent, 2004). Figure 4 shows that BB-M22 trend matches our analysis of the PSVM database somewhat better than BB18 and TK03, and that the inclination anomaly is well described by this zonal GAD based model. This is supported by a statistical analysis (Table 3) as $\chi^2$ does not exceed $\chi^2_{95}$. TK03, BB18 and BB-M22 assert a GAD-like field in which only the dipole coefficient, $g_1^0$, is held at a non-zero average. For the last 10 million years, these GAD based GGP models did not describe the inclination anomaly well, motivating Bono et al. (2020) to create BB18.Z3 with non-zero mean $g_2^0$ and $g_3^0$ coefficients. This zonally non-GAD model better described the shape of the inclination anomaly datapoints for PSV10, suggesting non-GAD features are needed to describe the magnetic field behavior in the last 10 million years. For PSVM, these zonal non-GAD features are not needed to provide a good description of the inclination anomaly behavior.

## 4. Discussion

### 4.1. Model G fit

The Model G fit does a relatively poor job of describing the VGP dispersion versus latitude in PSVM. This was similarly seen for the PSV10 database by Doubrovine et al. (2019). Regardless, the *a* and *b* values may still provide important information about the behavior of the field (Biggin et al., 2020). The *a* value is much more precisely defined than the *b* value and the scatter in VGP dispersion estimates makes it difficult to comment on the strength of the latitudinal dependency in VGP dispersion data for the Miocene. In predicting VGP dispersion at the equator, the Model G parameter *a* provides important information on the minimum expected variability of the Earth's magnetic field during the Miocene. Table 2 shows *a* values that vary depending on the applied selection criteria and cut-off.

They are all substantially higher than the Model G prediction based on PSV10 according to Doubrovine et al. (2019) and, in most cases, the differences are statistically significant. In the study of Doubrovine et al. (2019), the PSV10 database (Cromwell et al., 2018) was used to provide a new Model G prediction for the magnetic field, where $a_{PSV10}$ = 11.3° (10.2° – 12.6°). These uncertainty bounds do not overlap with those of the Model G prediction for our preferred subset of PSVM, where $a_{PSVM}$ = 15.7° (13.0° – 18.7°). None of the subsets have a lower average *a* value than $CS7_{VD}$ with the exception of $CS15_{VD}$, which has an uncertainty bound (10.8° - 19.1°) that is substantially wider than the other subsets.

*Table 4; Different databases for different eras with their Model G predictions. The Age is reported in Ma, Ng reports the number of Localities or Bins used for the Model G prediction. Model G parameters a and b with their 95% uncertainties are reported for each Database, as well as the study that the numbers were taken from. *Note that the recalculation of PSV10a was done in this study by not applying the envelope criteria suggested by Deenen et al. (2011), but the database PSV10a came from de Oliveira et al. (2021), and that the calculation of Model G parameters for 0-5 Ma was done by Doubrovine et al. (2019), but the database came from Opdyke et al. (2015).*

| Database | Age | $N_g$ | *a*(°) | b | Study reference |
|---|---|---|---|---|---|
| PSV – 0-5* | 0 – 5 | 29 | 11.6 +1.4/-1.3 | 0.26 +0.03/-0.04 | Doubrovine et al. (2019) |
| PSV10 (Bins) | 0 – 10 | 16 | 11.3 +1.3/-1.1 | 0.27 +0.04/-0.08 | Doubrovine et al. (2019) |
| PSV10 (Localities) | 0 – 10 | 51 | 11.3 +1.9/-1.6 | 0.26 +0.04/-0.05 | Sprain et al. (2019) |
| PSV10a (Studies) | 0 – 10 | 70 | 12.2 +1.5/-1.3 | 0.22 +0.04/-0.07 | de Oliveira et al. (2021) |
| PSV10a recalculated* | 0 – 10 | 80 | 11.1 +1.5/-1.5 | 0.25 +0.04/-0.05 | This study |
| PSVM – $CS7_{VD}$ | 5 – 23 | 23 | 15.7 +3.0/-2.7 | 0.23 +0.14/-0.23 | This study |
| PSVM – $CS2_{VD}$ | 5 – 23 | 31 | 17.4 +3.2/-3.4 | 0.21 +0.14/-0.21 | This study |
| PSVM – $CS7_{VD}$ (Bins) | 5 – 23 | 9 | 15.9 +2.9/-3.2 | 0.28 +0.07/-0.28 | This study |
| PSV – CNS | 84 – 126 | 19 | 10.7 +2.2/-2.4 | 0.21 +0.05/-0.16 | Doubrovine et al. (2019) |
| PSV – Pre CNS | 126 – 198 | 20 | 12.7 +1.9/-2.7 | 0.13 +0.13/-0.13 | Doubrovine et al. (2019) |
| PSV – Post PCRS | 200 – 264 | 21 | 14.2 +3.9/-0.9 | 0.15 +0.12/-0.10 | Handford et al. (2021) |
| PSV – PCRS | 265 – 318 | 16 | 5.5 + 3.1/-4.7 | 0.33 + 0.09/-0.09 | Handford et al. (2021) |

The comparison between the Model G prediction by Doubrovine et al. (2019), hereafter referred to as Model $G_{D19}$, and our Model G prediction for the Miocene must be interpreted carefully due to differences in how VGP dispersion data are treated. Model $G_{D19}$ is based on the PSV10 database being binned in 10° latitude bins from which VGP dispersion was calculated, the criteria of at least 2 reversals per locality was not implemented for PSV10, and the criterion *n ≥ 4* (instead *of n ≥ 5*) was applied to the PSV10 database and therefore also to Model $G_{D19}$. Because of this incompatibility, the decision was made to compare the Model G prediction for our $CS2_{VD}$ subset, which has the same selection criteria as PSV10, with Model $G_{S19}$ the Model G prediction produced by Sprain et al. (2019). Sprain et al (2019) used the PSV10 database but divided in localities instead of 10° bins, allowing for a better comparison with our datasets. $CS2_{VD}$ gives an *a* value of 17.4° (14.0° – 20.6°), which is higher than the *a* value of Model $G_{S19}$, 11.3° (9.7° – 13.3°), strengthening our confidence that VGP dispersion in the

Miocene was significantly higher than in the past 10 Myrs (Sprain et al., 2019). For completeness, a Model G prediction was created for our preferred subset ($CS7_{vD}$), in 10° latitude bins. Locality #8 (Steens mountain, Jarboe et al., 2008) was excluded from this analysis as it has experienced local block rotation and can therefore not be combined with other localities in that latitude bin. This Model G fit (Table 4, Supplementary Material Figure S3, Table S3) has an *a* parameter of 15.9° (12.6° - 18.7°). An updated PSV database for the past 10 Myrs, PSV10a (de Oliveira et al., 2021), produced a higher *a* value of 12.2° (10.8° – 13.6°) than that of Model $G_{D19}$ and Model $G_{S19}$. However, to calculate the VGP dispersion, de Oliveira et al. (2021) added a criterion proposed by Deenen et al. (2011) defined by an envelope $A_{95}$, to eliminate outliers. To avoid the risk of neglecting valid large values in the Miocene dataset, we do not apply the envelope method proposed by Deenen et al. (2011) to our database, making comparison with PSV10a more difficult. We recalculated the *a* and *b* values for the Model G prediction based on PSV10a without the envelope applied (Table 4). This analysis did not show an increase in *a* relative to Model $G_{D19}$. The *a* value for the recalculated Model G prediction based on PSV10a is 11.1° (9.6° – 12.6°), which does not overlap with the 95% confidence bounds of the *a* values for the Model G prediction for PSVM. Table 4 gives an overview of the *a* and *b* values for the different Model G predictions.

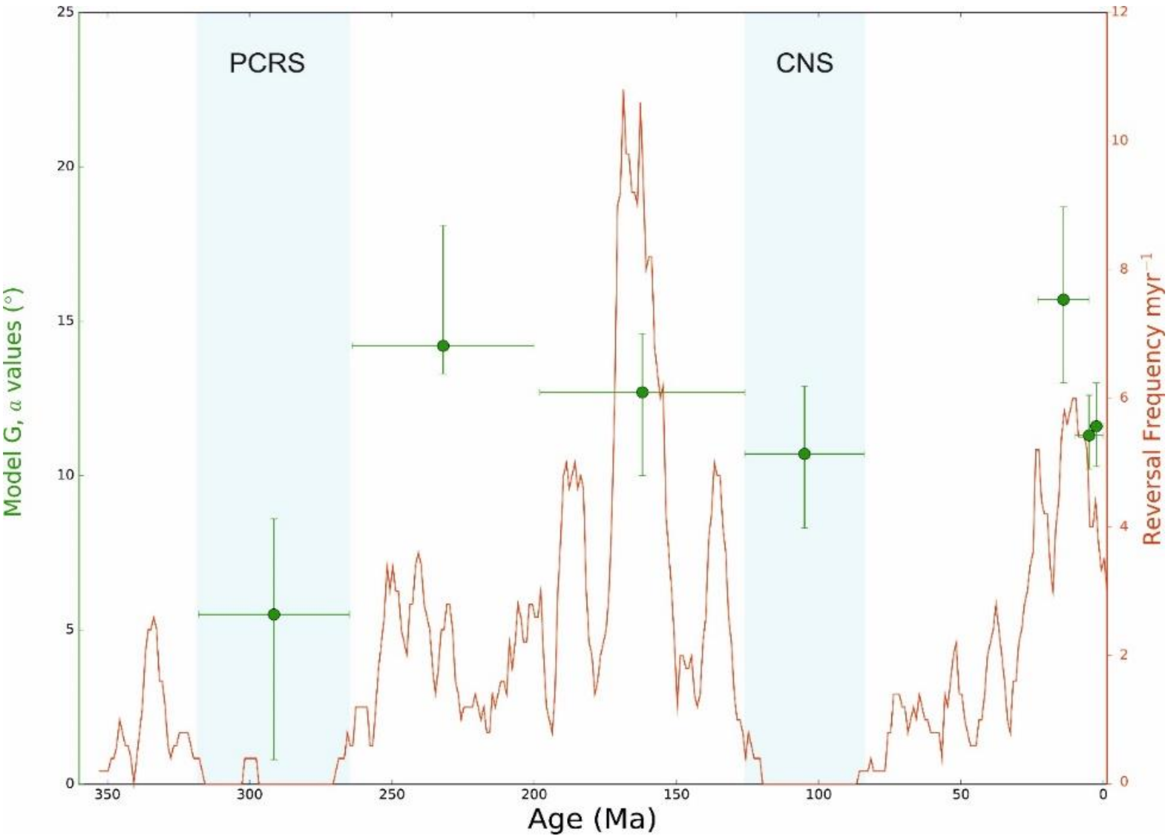


*Figure 5; The Model G parameter a in degrees vs Age. Each green dot with error bounds represents a PSV study with respective Model G prediction. The highlighted eras are the superchrons: CNS = Cretaceous Super Chron, PCRS = In orange the reversal frequency (calculated from Ogg. 2020) is presented for each Myrs, averaged over 5 myr.*

## 4.2. Comparison with different eras

Included in Table 4 are a selection of PSV studies performed in other time intervals. For the last 5 Ma specifically, several different databases and updates have been compiled, but the most recent was by Opdyke et al. (2015), which was used by Doubrovine et al. (2019) to calculate a Model G prediction for the past 5 Myrs. For the Cretaceous and Jurassic (CNS and Pre-CNS, respectively), an updated database was published by Doubrovine et al. (2019). For the Permian-Carboniferous Reversed Superchron (PCRS) multiple PSV studies have been published (Handford et al., 2021; de Oliveira et al., 2018); Handford et al. (2021) also reported on PSV in the Triassic (Post-PCRS). Table 4 and Figure 5 show the *a* parameter values for the most recent Model G predictions published for different time periods. The equatorial VGP dispersion obtained for the Miocene is higher than that of any recently published Model G predictions.

## 4.3. Implications for core processes in the Deep Earth during the Miocene

The high equatorial VGP dispersion of our preferred compilation reveals information about the geodynamo behavior in the Miocene. An analysis of a large and diverse set of geodynamo simulations (Biggin et al., 2020) has shown a clear relationship between the equatorial VGP dispersion (Model G parameter *a*) and the ratio between the dipolar and non-dipolar contributions of the geomagnetic field (AD/NAD). This relationship can be described by the equation:

$$\log\left(\frac{AD}{NAD}\right) \approx k_1 \times \log a + k_2 \tag{4}$$

Where AD/NAD represents the relative dipolarity, *a* is the equatorial VGP dispersion parameter for Model G, and $k_1$ and $k_2$ are the empirically obtained values -2.26 and 3.44, respectively (Biggin et al., 2020). Equation 4 gives our preferred subset of PSVM (*a* = 15.7° +3.0/-2.7), an AD/NAD estimate of 5.5 (+2.9/-1.8), which falls within the range that is described by Biggin et al. (2020) as Earth-like (3.5 – 45.0). It has previously been claimed (McFadden et al., 1991; Franco et al., 2019) that the ratio of Model G parameters b/a has an inverse relationship to the reversal frequency of the field at that time (Franco et al., 2019). Due to the wide range of *b* values recovered by our analyses, we are not able to comment on the validity of their hypothesis. Our low AD/NAD value nevertheless suggests a higher contribution of the non-dipolar geomagnetic field structures in the Miocene compared to most other eras, and the Miocene does show a higher reversal rate compared to the last 10 Myrs. We argue that the higher equatorial VGP dispersion in the Miocene is sufficient reason to suggest that the field in the Miocene was structurally less stable than in other eras, especially than in the past 5 Myrs. In Earth-like geodynamo simulations, equatorial VGP dispersion increases with Rayleigh number reflecting more vigorous convection in the outer core destabilizing the magnetic field (Meduri et al., 2021).

Convectional vigor is enhanced by elevating CMB heat flow, itself a consequence of decreased temperatures and/or increased thermal conductivity of the lowermost mantle. While we cannot rule out other causes of destabilization, our study is consistent with the idea that outer core flow was substantially more vigorous during the Miocene than it has been in most other eras. This could potentially have been a consequence of an increased flux of cold material into the lowermost mantle triggered by enhanced subduction at some earlier time (Hounslow et al., 2018).

## 5. Conclusions

We have compiled a new data set, PSVM, of high-quality paleodirectional data from the Miocene. The database includes 1,454 directions from 42 studies, divided in 44 different localities. The database has been used to perform statistical analyses on the behavior of the magnetic field in the Miocene. The observations of VGP dispersion versus latitude, and the Model G, BB-M22 and BB-M22.Z3 fits to them, suggest that the field did not behave similarly to the past 10 Myrs. The Model G descriptions for each version of the database do not strongly constrain the latitude dependence of VGP dispersion. The *b* values of the Model G predictions have 95% confidence bounds that extend to zero, preventing the possibility of no latitude dependence from being excluded. The *a* values for our Model G predictions yielded statistically significant results and show higher values than for the PSV10 and PSV10a compilations (Cromwell et al., 2018; de Oliveira et al., 2021). This suggests that on average the Miocene experienced a geomagnetic field which was less stable, and less dipolar compared to the average of the past 10 Myrs. These findings may imply an outer core that was convecting more vigorously.

## 6. Acknowledgements

This work was supported by The Leverhulme Trust (RL-2016-80) and the Natural Environment Research Council (NE/T012463/1). RKB acknowledges support from The Leverhulme Trust Early Career Fellowship (ECF-2020-617). The complete database has been made available as a supplementary material to this paper.

## 7. References

Argus, D. F., Gordon, R. G., & Demets, C. (2011). Geologically current motion of 56 plates relative to the no-net-rotation reference frame. *Geochemistry, Geophysics, Geosystems*, *12*(11). https://doi.org/10.1029/2011GC003751

Avigad, D., Baer, G., & Heimann, A. (1998). Block rotations and continental extension in the central Aegean Sea: palaeomagnetic and structural evidence from Tinos and Mykonos (Cyclades, Greece). *Earth and Planetary Science Letters*, *157*(98), 23–40.

Biggin, A. J., van Hinsbergen, D. J. J., Langereis, C. G., Straathof, G. B., & Deenen, M. H. L. (2008). Geomagnetic secular variation in the Cretaceous Normal Superchron and in the Jurassic. *Physics of the Earth and Planetary Interiors*, *169*(1–4), 3–19. https://doi.org/10.1016/j.pepi.2008.07.004

Biggin, A. J., Strik, G. H. M. A., & Langereis, C. G. (2009). The intensity of the geomagnetic field in the late-Archaean: New measurements and an analysis of the updated IAGA palaeointensity database. *Earth, Planets and Space*, *61*(1), 9–22. https://doi.org/10.1186/BF03352881

Biggin, A. J., Piispa, E. J., Pesonen, L. J., Holme, R., Paterson, G. A., Veikkolainen, T., & Tauxe, L. (2015). Palaeomagnetic field intensity variations suggest Mesoproterozoic inner-core nucleation. *Nature*, *526*(7572), 245–248. https://doi.org/10.1038/nature15523

Biggin, A. J., Bono, R. K., Meduri, D. G., Sprain, C. J., Davies, C. J., Holme, R., & Doubrovine, P. V. (2020). Quantitative estimates of average geomagnetic axial dipole dominance in deep geological time. *Nature Communications*, *11*(1), 1–9. https://doi.org/10.1038/s41467-020-19794-7

Bono, R. K., Biggin, A. J., Holme, R., Davies, C. J., Meduri, D. G., & Bestard, J. (2020). Covariant Giant Gaussian Process Models With Improved Reproduction of Palaeosecular Variation. *Geochemistry, Geophysics, Geosystems*, *21*(8). https://doi.org/10.1029/2020GC008960

Bono, R. K., Paterson, G. A., van der Boon, A., Engbers, Y. A., Michael Grappone, J., Handford, B., et al. (2022). The PINT database: a definitive compilation of absolute palaeomagnetic intensity determinations since 4 billion years ago. *Geophysical Journal International*, *229*(1), 522–545. https://doi.org/10.1093/gji/ggab490

Brandt, D., Constable, C., & Ernesto, M. (2020). Giant Gaussian process models of geomagnetic palaeosecular variation: A directional outlook. *Geophysical Journal International*, *222*(3), 1526–1541. https://doi.org/10.1093/gji/ggaa258

Caccavari, A., Calvo-Rathert, M., Goguitchaichvili, A., Soler, V., Huaiyu, H., & Vegas, N. (2015). An integrated palaeomagnetic, palaeointensity and40Ar/39Ar investigation on a miocene polarity transition recorded in a lava sequence in la Gomera, Canary Islands. *Geophysical Journal International*, *200*(3), 1297–1316. https://doi.org/10.1093/gji/ggu481

Calderone, G. J., Butler, R. F., & Acton, G. D. (1990). Paleomagnetism of Middle Miocene volcanic rocks in the Mojave-Sonora Desert region of western Arizona and southeastern California. *Journal of Geophysical Research*, *95*(B1), 625–647. https://doi.org/10.1029/JB095iB01p00625

Carracedo, J. C., & Soler, V. (1995). Anomalously shallow palaeomagnetic inclinations and the question of the age of the Canarian Archipelago. *Geophysical Journal International*, *122*(2), 393–406. https://doi.org/10.1111/j.1365-246X.1995.tb07003.x

Constable, C. G., & Johnson, C. L. (1999). Anisotropic paleosecular variation models: Implications for geomagnetic field observables. *Physics of the Earth and Planetary Interiors*, *115*(1), 35–51. https://doi.org/10.1016/S0031-9201(99)00065-5

Constable, C. G., & Parker, R. L. (1988). Statistics of the geomagnetic secular variation for the past 5 m.y. *Journal of Geophysical Research*, *93*(B10). https://doi.org/10.1029/jb093ib10p11569

Cromwell, G., Johnson, C. L., Tauxe, L., Constable, C. G., & Jarboe, N. A. (2018). PSV10: A Global Data Set for 0–10 Ma Time-Averaged Field and Paleosecular Variation Studies. *Geochemistry, Geophysics, Geosystems*, *19*(5), 1533–1558. https://doi.org/10.1002/2017GC007318

Deenen, M. H. L., Langereis, C. G., van Hinsbergen, D. J. J., & Biggin, A. J. (2011). Geomagnetic secular variation and the statistics of palaeomagnetic directions. *Geophysical Journal International*, *186*(2), 509–520. https://doi.org/10.1111/j.1365-246X.2011.05050.x

Dominguez, A. R., & Van der Voo, R. (2014). Secular variation of the middle and late Miocene geomagnetic field recorded by the Columbia River Basalt Group in Oregon, Idaho and Washington, USA. *Geophysical Journal International*, *197*(3), 1299–1320. https://doi.org/10.1093/gji/ggt487

Døssing, A., Riishuus, M. S., Mac Niocaill, C., Muxworthy, A. R., & Maclennan, J. (2020). Late Miocene to late Pleistocene geomagnetic secular variation at high northern latitudes. *Geophysical Journal International*, *222*(1), 86–102. https://doi.org/10.1093/gji/ggaa148

Doubrovine, P. V., Veikkolainen, T., Pesonen, L. J., Piispa, E., Ots, S., Smirnov, A. V., et al. (2019). Latitude Dependence of Geomagnetic Paleosecular Variation and its Relation to the Frequency of Magnetic Reversals: Observations From the Cretaceous and Jurassic. *Geochemistry, Geophysics, Geosystems*, *20*(3), 1240–1279. https://doi.org/10.1029/2018GC007863

Duarte, A. V., Böhnel, H., & Yutsis, V. (2015). Paleomagnetism of the Miocene Jantetelco Granodiorites and Tepexco Volcanic Group and inferences for crustal block rotations in central Mexico - Reevaluation. *Tectonophysics*, *658*, 117–127. https://doi.org/10.1016/j.tecto.2015.07.014

Engbers, Y. A., Biggin, A. J., & Bono, R. K. (2020). Elevated paleomagnetic dispersion at Saint Helena suggests long-lived anomalous behavior in the South Atlantic. *Proceedings of the National*

*Academy of Sciences of the United States of America*, *117*(31), 18258–18263. https://doi.org/10.1073/pnas.2001217117

Engbers, Y. A., Grappone, J. M., Mark, D. F., & Biggin, A. J. (2022). Low paleointensities and Ar/Ar ages from Saint Helena provide evidence for recurring magnetic field weaknesses in the South Atlantic. *Journal of Geophysical Research: Solid Earth*, 1–14. https://doi.org/10.1029/2021jb023358

Fisher, R. (1953). Dispersion on a Sphere. *Proceedings of the Royal Society A: Mathematical, Physical and Engineering Sciences*, *217*(1130), 295–305. https://doi.org/10.1098/rspa.1953.0064

Franco, D. R., de Oliveira, W. P., Freitas, F. B. V. de, Takahashi, D., da Ponte Neto, C. F., & Peixoto, I. M. C. (2019). Paleomagnetic Evidence for Inverse Correspondence between the Relative Contribution of the Axial Dipole Field and CMB Heat Flux for the Past 270 Myr. *Scientific Reports*, *9*(1), 1–8. https://doi.org/10.1038/s41598-018-36494-x

Garza, R. S. M., van Hinsbergen, D. J. J., Rogers, R. D., Ganerød, M., & Dekkers, M. J. (2012). The Padre Miguel Ignimbrite Suite, central Honduras: Paleomagnetism, geochronology, and tectonic implications. *Tectonophysics*, *574–575*, 144–157. https://doi.org/10.1016/j.tecto.2012.08.013

Glen, J. M. G., Valet, J. P., Soler, V., Renne, P. R., & Elmaleh, A. (2003). A Neogene geomagnetic polarity transition record from lavas of the Canary Islands, Spain: Episodic volcanism and/or metastable transitional fields? *Geophysical Journal International*, *154*(2), 426–440. https://doi.org/10.1046/j.1365-246X.2003.01966.x

Goguitchaichvili, A., Chauvin, A., Roperch, P., Prévot, M., Aguirre, L., & Vergara, M. (2000). Palaeomagnetism of the Miocene Farellones formation (Chile). *Geophysical Journal International*, *140*(2), 357–373. https://doi.org/10.1046/j.1365-246x.2000.00022.x

Goguitchaichvili, Avto, González, J. A., Pluhar, C. J., Alvavaldivia, L., Elguera, J. R., RuizMartínez, V. C., et al. (2011). A comprehensive rock-magnetic, paleomagnetic, paleointensity and geochronologic study along the western Trans-Mexican volcanic belt: Geodynamic and geomagnetic implications. *Geofisica Internacional*, *50*(2), 227–254. https://doi.org/10.22201/igeof.00167169p.2011.50.2.141

Hagstrum, J. T., Sawlan, M. G., Hausback, B. P., Smith, J. G., & Gromme, C. S. (1987). Miocene paleomagnetism and tectonic setting of the Baja California Peninsula, Mexico. *Journal of Geophysical Research*, *92*(B3), 2627–2639. https://doi.org/10.1029/JB092iB03p02627

Handford, B. T., Biggin, A. J., Haldan, M. M., & Langereis, C. G. (2021). Analysing Triassic and Permian Geomagnetic Palaeosecular Variation and the Implications for Ancient Field Morphology. *Geochemistry, Geophysics, Geosystems*. https://doi.org/10.1029/2021gc009930

Hansma, J., & Tohver, E. (2018). Palaeomagnetism of mid-Miocene leucitite volcanics in eastern Australia. *Geophysical Journal International*, *215*(1), 303–313. https://doi.org/10.1093/gji/ggy281

Henry, B., & Plessard, C. (1997). New palaeomagnetic results from the Kerguelen Islands. *Geophysical Journal International*, *128*(1), 73–83. https://doi.org/10.1111/j.1365-246X.1997.tb04072.x

Hoshi, H., & Sano, M. (2013). Paleomagnetic constraints on Miocene rotation in the Central Japan Arc. *Island Arc*, *22*(2), 197–213. https://doi.org/10.1111/iar.12022

Hoshi, H., & Teranishi, Y. (2007). Paleomagnetism of the Ishikoshi Andesite: A Middle Miocene paleomagnetic pole for northeastern Japan and tectonic implications. *Earth, Planets and Space*, *59*(7), 871–878. https://doi.org/10.1186/BF03352749

Hoshi, H., & Yokoyama, M. (2001). Paleomagnetism of miocene dikes in the Shitara basin and the tectonic evolution of central Honshu, Japan. *Earth, Planets and Space*, *53*(7), 731–739. https://doi.org/10.1186/BF03352401

Irving, E., Baker, J., Wynne, P. J., Hamilton, T. S., & Wingate, M. T. D. (2000). Evolution of the Queen Charlotte Basin: Further paleomagnetic evidence of Tertiary extension and tilting. *Tectonophysics*, *326*(1–2), 1–22. https://doi.org/10.1016/S0040-1951(00)00143-8

Jarboe, N. A., Coe, R. S., Renne, P. R., Glen, J. M. G., & Mankinen, E. A. (2008). Quickly erupted volcanic sections of the Steens Basalt, Columbia River Basalt Group: Secular variation, tectonic rotation, and the Steens Mountain reversal. *Geochemistry, Geophysics, Geosystems*, *9*(11). https://doi.org/10.1029/2008GC002067

Johnson, C. L., & Constable, C. G. (1996). Palaeosecular variation recorded by lava flows over the past five million years. *Philosophical Transactions of the Royal Society of London*, (Series A, 354(1704)), 89–141.

Johnson, C. L., & McFadden, P. (2007). Time-Averaged Field and Paleosecular Variation. *Treatise on Geophysics*, *5*, 417–453. https://doi.org/10.1016/B978-044452748-6.00096-1

Johnson, C. L., & McFadden, P. (2015). *The Time-Averaged Field and Paleosecular Variation*. *Treatise on Geophysics: Second Edition* (Vol. 5). Published by Elsevier Inc. https://doi.org/10.1016/B978-

0-444-53802-4.00105-6

Johnson, C. L., Constable, C. G., Tauxe, L., Barendregt, R., Brown, L. L., Coe, R. S., et al. (2008). Recent investigations of the 0-5 Ma geomagnetic field recorded by lava flows. *Geochemistry, Geophysics, Geosystems*, *9*(4). https://doi.org/10.1029/2007GC001696

Kirschvink, J. L. (1980). The least-squares line and plane and the analysis of palaeomagnetic data. *Geophysical Journal of the Royal Astronomical Society*, *62*(3), 699–718. https://doi.org/10.1111/j.1365-246X.1980.tb02601.x

Leonhardt, R., & Soffel, H. C. (2002). A reversal of the Earth's magnetic field recorded in mid-Miocene lava flows of Gran Canaria: Paleointensities. *Journal of Geophysical Research: Solid Earth*, *107*(B11), EPM 5-1-EPM 5-11. https://doi.org/10.1029/2001jb000949

Leonhardt, R., & Soffel, H. C. (2006). The growth, collapse and quiescence of Teno volcano, Tenerife: New constraints from paleomagnetic data. *International Journal of Earth Sciences*, *95*(6), 1053–1064. https://doi.org/10.1007/s00531-006-0089-3

Leonhardt, R., Hufenbecher, F., Heider, F., & Soffel, H. C. (2000). High absolute paleointensity during a mid Miocene excursion of the Earth's magnetic field. *Earth and Planetary Science Letters*, *184*(1), 141–154. https://doi.org/10.1016/S0012-821X(00)00311-3

Leonhardt, R., Matzka, J., & Menor, E. A. (2003). Absolute paleointensities and paleodirections of miocene and pliocene lavas from Fernando de Noronha, Brazil. *Physics of the Earth and Planetary Interiors*, *139*(3–4), 285–303. https://doi.org/10.1016/j.pepi.2003.09.008

Lhuillier, F., & Gilder, S. A. (2019). Palaeomagnetism and geochronology of Oligocene and Miocene volcanic sections from Ethiopia: Geomagnetic variability in the Afro-Arabian region over the past 30 Ma. *Geophysical Journal International*, *216*(2), 1466–1481. https://doi.org/10.1093/gji/ggy517

Linder, J., & Leonhardt, R. (2009). Paleomagnetic full vector record of four consecutive Mid Miocene geomagnetic reversals. *Physics of the Earth and Planetary Interiors*, *177*(1–2), 88–101. https://doi.org/10.1016/j.pepi.2009.07.013

Mankinen, E. A. (2008). Paleomagnetic study of late miocene through pleistocene igneous rocks from the southwestern USA: Results from the historic collections of the U.S. geological survey menlo park laboratory. *Geochemistry, Geophysics, Geosystems*, *9*(5). https://doi.org/10.1029/2008GC001957

McElhinny, M. W., & McFadden, P. L. (1997). Palaeosecular variation over the past 5 Myr based on a new generalized database. *Geophysical Journal International*, *131*(2), 240–252. https://doi.org/10.1111/j.1365-246X.1997.tb01219.x

Mcfadden, P. L., Merrill, R. T., & Mcelhinny, M. W. (1988). Dipole / Quadrupole Family Modeling of Paleosecular Variation. *Journal of Geophysical Research*, *93*(7), 11583–11588.

Mcfadden, P. L., Merrill, R. T., Mcelhinny, M. W., & Lee, S. (1991). Reversals of the Earth's Magnetic Field and Temporal Variations of the Dynamo Families. *Journal of Geophysical Research*, *96*, 3923–3933.

Meduri, D. G., Biggin, A. J., Davies, C. J., Bono, R. K., Sprain, C. J., & Wicht, J. (2021). Numerical Dynamo Simulations Reproduce Paleomagnetic Field Behavior. *Geophysical Research Letters*, *48*(5), 1–10. https://doi.org/10.1029/2020GL090544

de Oliveira, W. P., Franco, D. R., Brandt, D., Ernesto, M., da Ponte Neto, C. F., Zhao, X., et al. (2018). Behavior of the paleosecular variation during the permian-carboniferous reversed superchron and comparisons to the low reversal frequency intervals since precambrian times. *Geochemistry, Geophysics, Geosystems*, *19*(4), 1035–1048. https://doi.org/10.1002/2017GC007262

de Oliveira, W. P., Hartmann, G. A., Terra-Nova, F., Brandt, D., Biggin, A. J., Engbers, Y. A., et al. (2021). Paleosecular Variation and the Time-Averaged Geomagnetic Field Since 10 Ma. *Geochemistry, Geophysics, Geosystems*, *22*(10). https://doi.org/10.1029/2021gc010063

Opdyke, N. D., Kent, D. V., Foster, D. A., & Huang, K. (2015). Paleomagnetism of Miocene volcanics on Sao Tome: Paleosecular variation at the Equator and a comparison to its latitudinal dependence over the last 5 Myr. *Geochemistry, Geophysics, Geosystems*, *16*(11), 3870–3882. https://doi.org/10.1002/2015GC005901

Otofuji, Y. -i, Itaya, T., & Matsuda, T. (1991). Rapid rotation of southwest Japan — palaeomagnetism and K-Ar ages of Miocene volcanic rocks of southwest Japan. *Geophysical Journal International*, *105*(2), 397–405. https://doi.org/10.1111/j.1365-246X.1991.tb06721.x

Otofuji, Y. I., Nishizawa, Y., Tamai, M., & Matsuda, T. (1997). Palaeomagnetic and chronological study of Miocene welded tuffs in the northern part of Central Japan: Tectonic implications for the latest stage of arc formation of Japan. *Tectonophysics*, *283*(1–4), 263–278. https://doi.org/10.1016/S0040-1951(97)00065-6

Pan, Y., Hill, M. J., & Zhu, R. (2005). Paleomagnetic and paleointensity study of an Oligocene-Miocene lava sequence from the Hannuoba Basalts in northern China. *Physics of the Earth and*

*Planetary Interiors*, *151*(1–2), 21–35. https://doi.org/10.1016/j.pepi.2004.12.004

Pearson, K. (1900). X. On the criterion that a given system of deviations from the probable in the case of a correlated system of variables is such that it can be reasonably supposed to have arisen from random sampling . *The London, Edinburgh, and Dublin Philosophical Magazine and Journal of Science*, *50*(302), 157–175. https://doi.org/10.1080/14786440009463897

Press, W. H., Teukolsky, S. A., Vetterling, W. T., & Flannery, B. P. (1992). *Numerical Recipes in C* (Vol. 76). Cambridge University Press.

Quidelleur, X., & Courtillot, V. (1996). On low-degree spherical harmonic models of paleosecular variation. *Physics of the Earth and Planetary Interiors*, *95*(1–2), 55–77. https://doi.org/10.1016/0031-9201(95)03115-4

Riisager, J., Perrin, M., Riisager, P., & Ruffet, G. (2000). Post-Miocene Pyroclastites, *105*, 883–896.

Roperch, P., Carlotto, V., Ruffet, G., & Fornari, M. (2011). Tectonic rotations and transcurrent deformation south of the Abancay deflection in the Andes of southern Peru. *Tectonics*, *30*(2). https://doi.org/10.1029/2010TC002725

Ruiz-Martínez, V. C., Osete, M. L., Vegas, R., Núñez-Aguilar, J. I., Urrutia-Fucugauchi, J., & Tarling, D. H. (2000). Palaeomagnetism of Late Miocene to Quaternary volcanics from the eastern segment of the Trans-Mexican Volcanic Belt. *Tectonophysics*, *318*(1–4), 217–233. https://doi.org/10.1016/S0040-1951(99)00313-3

Ruiz-Martínez, V. C., Urrutia-Fucugauchi, J., & Osete, M. L. (2010). Palaeomagnetism of the western and central sectors of the Trans-Mexican volcanic belt - implications for tectonic rotations and palaeosecular variation in the past 11 Ma. *Geophysical Journal International*, *180*(2), 577–595. https://doi.org/10.1111/j.1365-246X.2009.04447.x

Sherwood, G. J. (1988). Paleomagnetism and magnetostratigraphy of miocene volcanics in eastern otago and banks peninsula, New Zealand. *New Zealand Journal of Geology and Geophysics*, *31*(2), 207–224. https://doi.org/10.1080/00288306.1988.10417770

Sherwood, G. J. (1990). A paleomagnetic and rock magnetic study of Tertiary volcanics from the Vogelsberg (Germany). *Physics of the Earth and Planetary Interiors*, *62*(1–2), 32–45. https://doi.org/10.1016/0031-9201(90)90190-9

Smirnov, A. V., Tarduno, J. A., & Evans, D. A. D. (2011). Evolving core conditions ca. 2 billion years ago detected by paleosecular variation. *Physics of the Earth and Planetary Interiors*, *187*(3–4), 225–231. https://doi.org/10.1016/j.pepi.2011.05.003

Somoza, R., Singer, S., & Coira, B. (1996). Paleomagnetismo f upper Miocene ignimbritesa t the Puna: An analysis of vertical-axis rotations in the Central Andes. *Journal of Geophysical Research*, *101*(B5), 11,387-11,400.

Sprain, C. J., Biggin, A. J., Davies, C. J., Bono, R. K., & Meduri, D. G. (2019). An assessment of long duration geodynamo simulations using new paleomagnetic modeling criteria (QPM). *Earth and Planetary Science Letters*, *526*, 115758. https://doi.org/10.1016/j.epsl.2019.115758

Takahashi, M., Hoshi, H., & Yamamoto, T. (1999). Miocene counterclockwise rotation of the Abukuma Mountains, Northeast Japan. *Tectonophysics*, *306*(1), 19–31. https://doi.org/10.1016/S0040-1951(99)00044-X

Tauxe, L., & Kent, D. V. (2004). A simplified statistical model for the geomagnetic field and the detection of shallow bias in paleomagnetic inclinations: Was the ancient magnetic field dipolar? *Geophysical Monograph Series*, *145*, 101–115. https://doi.org/10.1029/145GM08

Ubangoh, R. U., Pacca, I. G., & Nyobe, J. B. (1998). Palaeomagnetism of the continental sector of the Cameroon Volcanic Line, West Africa. *Geophysical Journal International*, *135*(2), 362–374. https://doi.org/10.1046/j.1365-246X.1998.00635.x

Vandamme, D. (1994). A new method to determine paleosecular variation. *Physics of the Earth and Planetary Interiors*, *85*(1–2), 131–142. https://doi.org/10.1016/0031-9201(94)90012-4

Veikkolainen, T., & Pesonen, L. J. (2014). Palaeosecular variation, field reversals and the stability of the geodynamo in the Precambrian. *Geophysical Journal International*, *199*(3), 1515–1526. https://doi.org/10.1093/gji/ggu348

Vişan, M., Panaiotu, C. G., Necula, C., & Dumitru, A. (2016). Palaeomagnetism of the Upper Miocene-Lower Pliocene lavas from the East Carpathians: Contribution to the paleosecular variation of geomagnetic field. *Scientific Reports*, *6*(March), 1–7. https://doi.org/10.1038/srep23411

Zheng, Z., Tanaka, H., Tatsumi, Y., & Kono, M. (2002). Basalt platforms in Inner Mongolia and Hebei Province, northeastern China: New K-Ar ages, geochemistries, and revision of palaeomagnetic results. *Geophysical Journal International*, *151*(2), 654–662. https://doi.org/10.1046/j.1365-246X.2002.01788.x

AGU PUBLICATIONS

*G*[3] | *Geochemistry, Geophysics, Geosystems*

Supporting Information for

# PSVM: A global database for the Miocene indicating elevated paleosecular variation relative to the last 10 Myrs.

Y. A. Engbers[1], R. K. Bono[1,2] and A. J. Biggin[1]

1. Geomagnetism Laboratory, Department of Earth, Ocean and Ecological Sciences, University of Liverpool, Liverpool L69 7ZE, United Kingdom

2. Earth Materials Laboratory, Department of Earth, Ocean and Atmospheric Science, Florida State University, Tallahassee, Florida 32306, United States

## Contents of this file

Text S1
Figures S1 to S4
Table S1 to S3

## Additional Supporting Information (Files uploaded separately)

Captions for Dataset S1

## **Text S1 Serial Correlation:**

When lava flows erupt rapidly, multiple stacked flows might represent the same snapshot of the Earth's magnetic field. In a PSV study, this serial correlation (SC) can produce overrepresentation of short time periods leading to underestimation of the VGP dispersion associated with the secular variation (Biggin et al., 2008). To check for serial correlation in the studies, a common true mean direction (CTMD) test is commonly used (Tauxe, 2010; Watson, 1956). For this test, the individually measured directions per sample are needed which are often not provided in the literature. To overcome this problem, bootstrapped parametric sampling (creating a possible set of sample level directions to create the mean-direction given, with the known number of samples, with the known *k* value, Tauxe et al., 1991) was performed for every site mean after which the Watson test of randomness was performed on every two stacked sites. This process was repeated 10000 times to compensate for the randomness of parametric sampling. Whenever two or three sites were serially correlated, the site(s) with a higher $\alpha_{95}$ value was (were) ignored in the SC corrected database ($PSVM^{SC}$). When 4 sites or more were stacked and serially correlated, the bottom and top site were included and the middle sites ignored. In total 301 sites (21%) were excluded from $PSVM^{SC}$. This sequence was repeated for each database with different applied selection criteria (*k* and *n*) as discussed in the previous section.

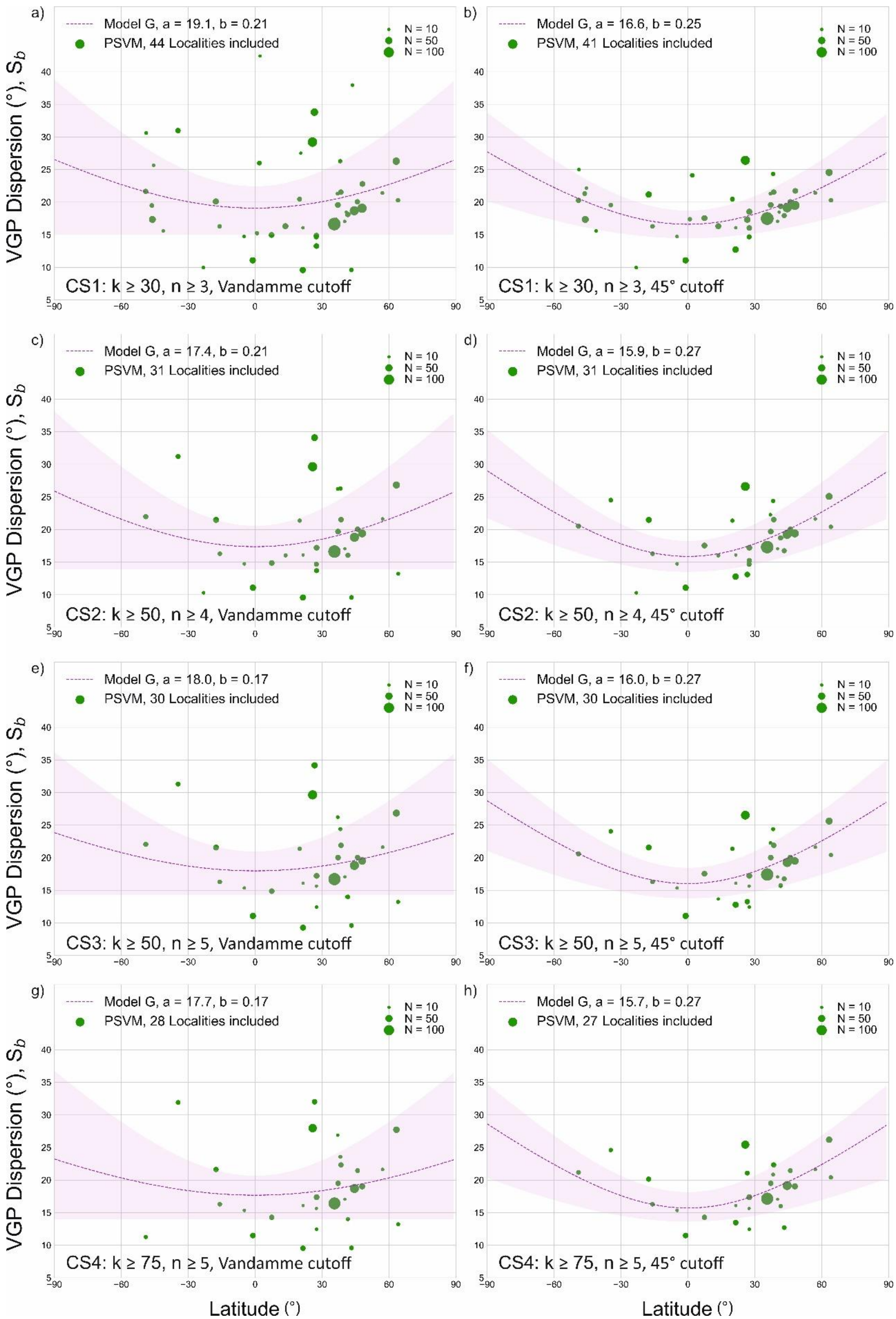

a)
Model G, a = 19.1, b = 0.21
PSVM, 44 Localities included
CS1: k ≥ 30, n ≥ 3, Vandamme cutoff
b)
Model G, a = 16.6, b = 0.25
PSVM, 41 Localities included
CS1: k ≥ 30, n ≥ 3, 45° cutoff
c)
Model G, a = 17.4, b = 0.21
PSVM, 31 Localities included
CS2: k ≥ 50, n ≥ 4, Vandamme cutoff
d)
Model G, a = 15.9, b = 0.27
PSVM, 31 Localities included
CS2: k ≥ 50, n ≥ 4, 45° cutoff
e)
Model G, a = 18.0, b = 0.17
PSVM, 30 Localities included
CS3: k ≥ 50, n ≥ 5, Vandamme cutoff
f)
Model G, a = 16.0, b = 0.27
PSVM, 30 Localities included
CS3: k ≥ 50, n ≥ 5, 45° cutoff
g)
Model G, a = 17.7, b = 0.17
PSVM, 28 Localities included
CS4: k ≥ 75, n ≥ 5, Vandamme cutoff
h)
Model G, a = 15.7, b = 0.27
PSVM, 27 Localities included
CS4: k ≥ 75, n ≥ 5, 45° cutoff
N = 10
N = 50
N = 100
VGP Dispersion (°), $S_b$
Latitude (°)

**Figure S1.** VGP dispersion versus latitude per locality in PSVM with different selection criteria (CS 1 to 4 in the main manuscript and Table S1) and cut-offs. Green dots represent the localities from PSVM and their size represents the number of sites included in that locality (N). The pink dashed line represents the Model G prediction for this specific situation and the pink shaded area represents the 95% confidence bounds on that Model G prediction. Subfigures a and b show PSVM with selection criteria set 1 (CS1). Subfigures c and d show subset CS2. Subfigures e and f show subset CS3 and subfigures g and h show subset CS4. Subfigures a, c, e and g show VGP dispersion with a Vandamme cut-off (1994), where subfigures b, d, f and h show the VGP dispersion with a 45° cut-off.

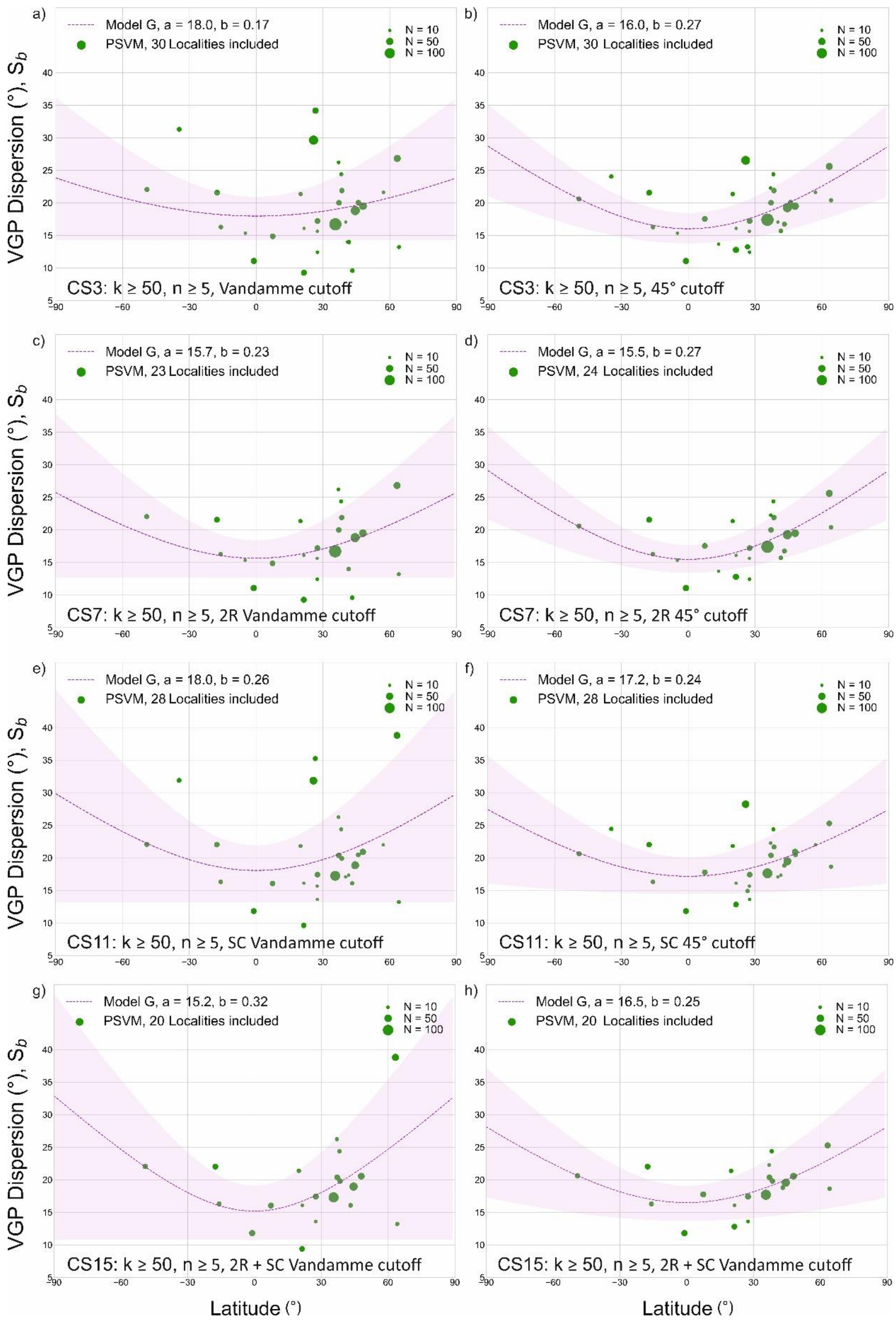

a)
Model G, a = 18.0, b = 0.17
PSVM, 30 Localities included
CS3: k ≥ 50, n ≥ 5, Vandamme cutoff
b)
Model G, a = 16.0, b = 0.27
PSVM, 30 Localities included
CS3: k ≥ 50, n ≥ 5, 45° cutoff
c)
Model G, a = 15.7, b = 0.23
PSVM, 23 Localities included
CS7: k ≥ 50, n ≥ 5, 2R Vandamme cutoff
d)
Model G, a = 15.5, b = 0.27
PSVM, 24 Localities included
CS7: k ≥ 50, n ≥ 5, 2R 45° cutoff
e)
Model G, a = 18.0, b = 0.26
PSVM, 28 Localities included
CS11: k ≥ 50, n ≥ 5, SC Vandamme cutoff
f)
Model G, a = 17.2, b = 0.24
PSVM, 28 Localities included
CS11: k ≥ 50, n ≥ 5, SC 45° cutoff
g)
Model G, a = 15.2, b = 0.32
PSVM, 20 Localities included
CS15: k ≥ 50, n ≥ 5, 2R + SC Vandamme cutoff
h)
Model G, a = 16.5, b = 0.25
PSVM, 20 Localities included
CS15: k ≥ 50, n ≥ 5, 2R + SC Vandamme cutoff
N = 10
N = 50
N = 100
VGP Dispersion (°), S_b
Latitude (°)

**Figure S2.** VGP dispersion versus latitude per locality in PSVM with different selection criteria (CS3, 7, 11, 15 in the main manuscript and Table S1) and cut-offs. Green dots represent the localities from PSVM and their size represents the number of sites included in that locality (N). The pink dashed line represents the Model G prediction for this specific situation and the pink shaded area represents the 95% confidence bounds on that Model G prediction. All of the subfigures show different variations of PSVM with k ≥ 50 and n ≥ 5. Subfigures a and b show PSVM (CS3), c and d show $PSVM^{2R}$ (CS7). Subfigures e and f show $PSVM^{SC}$ (CS11) and subfigures g and h show $PSVM^{SC\text{-}2R}$ (CS15). Subfigures a, c, e and g show VGP dispersion with a Vandamme cut-off (1994), where subfigures b, d, f and h show the VGP dispersion with a 45° cutoff.

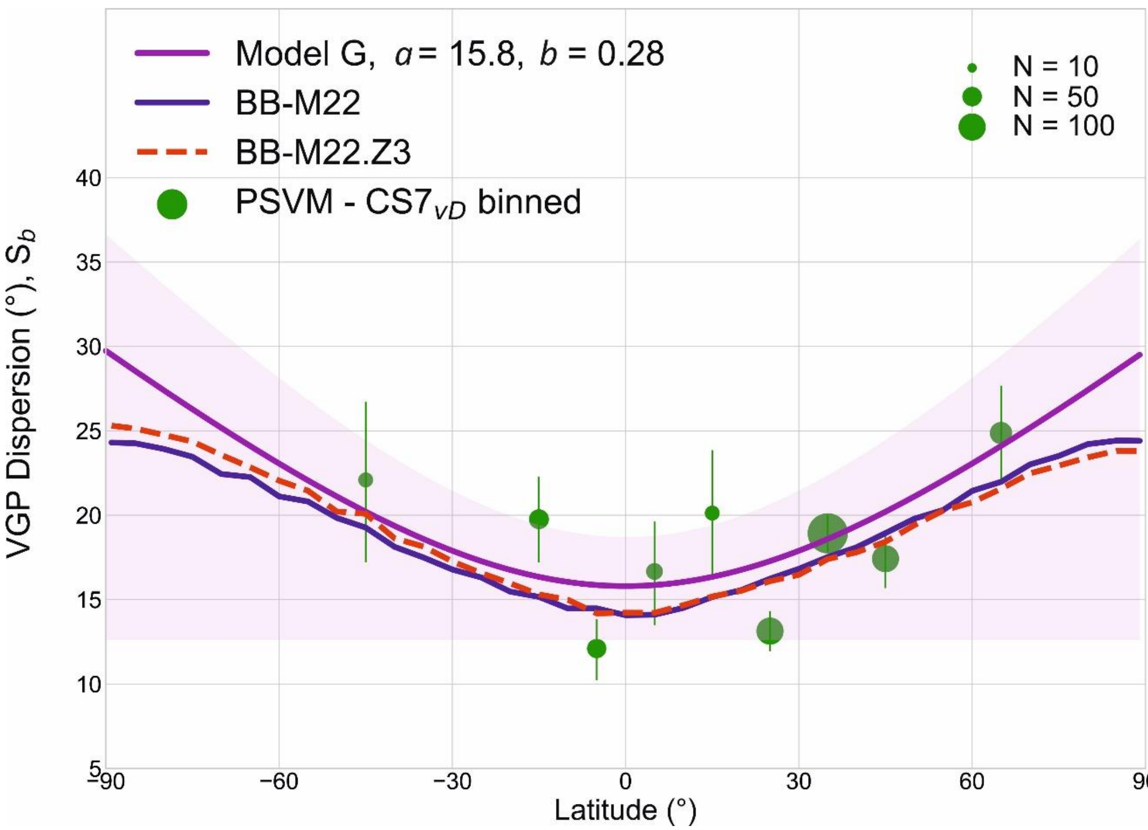


**Figure S3.** VGP dispersion versus latitude per 10° latitude bin in PSVM ($CS7_{vD}$, excluding locality #8 due to local block rotation). Green dots represent the bins from PSVM with their error margin, and the size of the dot represents the number of sites included in that bin (N). The pink dashed line represents the Model G prediction for this specific situation and the pink shaded area represents 95% confidence bounds on that Model G prediction. The blue line and red dashed line represent the predictions from BB-M22 and BB-M22.Z3 based on the PSVM localities (main text).

| | Selection Criteria | | | | *Vandamme cut-off* | | *45° cut-off* | |
|---|---|---|---|---|---|---|---|---|
| PSVM subset: | *n* | *k* | 2R | SC | *a* values | *b* values | *a* values | *b* values |
| **CS1** | **≥ 3** | **> 30** | **N** | **N** | **19.1 +3.3/-4.1** | **0.21 +0.15/-0.20** | **16.6 +2.1/-2.2** | **0.25 +0.07/-0.09** |
| **CS2** | **≥ 4** | **> 50** | **N** | **N** | **17.4 +3.3/-3.4** | **0.21 +0.14/-0.21** | **15.9 +2.4/-2.3** | **0.27 +0.07/-0.08** |
| **CS3** | **≥ 5** | **> 50** | **N** | **N** | **18.0 +3.0/-3.7** | **0.17 +0.15/-0.17** | **16.0 +2.4/-2.2** | **0.27 +0.07/-0.09** |
| **CS4** | **≥ 5** | **> 75** | **N** | **N** | **17.7 +2.9/-3.7** | **0.17 +0.17/-0.17** | **15.7 +2.4/-2.1** | **0.27 +0.06/-0.10** |
| CS5 | ≥ 3 | > 30 | Y | N | 18.3 +3.4/-4.0 | 0.19 +0.15/-0.19 | 16.7 +2.0/-2.1 | 0.25 +0.07/-0.09 |
| CS6 | ≥ 4 | > 50 | Y | N | 15.7 +2.5/-2.7 | 0.23 +0.14/-0.23 | 15.8 +2.0/-2.0 | 0.27 +0.07/-0.08 |
| **CS7** | **≥ 5** | **> 50** | **Y** | **N** | **15.7 +2.7/-3.0** | **0.23 +0.14/-0.23** | **15.5 +2.2/-2.1** | **0.27 +0.07/-0.09** |
| CS8 | ≥ 5 | > 75 | Y | N | 15.3 +2.5/-2.9 | 0.20 +0.15/-0.20 | 14.4 +1.9/-1.8 | 0.28 +0.06/-0.09 |
| CS9 | ≥ 3 | > 30 | N | Y | 19.5 +3.9/-4.7 | 0.29 +0.17/-0.28 | 17.3 +2.2/-2.3 | 0.24 +0.08/-0.11 |
| CS10 | ≥ 4 | > 50 | N | Y | 17.7 +4.1/-4.5 | 0.29 +0.18/-0.29 | 17.2 +2.7/-2.4 | 0.24 +0.08/-0.13 |
| **CS11** | **≥ 5** | **> 50** | **N** | **Y** | **18.0 +3.9/-4.8** | **0.26 +0.18/-0.26** | **17.2 +2.9/-2.7** | **0.24 +0.16/-0.09** |
| CS12 | ≥ 5 | > 75 | N | Y | 17.5 +4.0/-4.5 | 0.26 +0.18/-0.25 | 16.6 +2.9/-2.5 | 0.25 +0.08/-0.14 |
| CS13 | ≥ 3 | > 30 | Y | Y | 18.5 +4.0/-4.6 | 0.28 +0.17/-0.28 | 17.2 +2.1/-2.2 | 0.25 +0.09/-0.11 |
| CS14 | ≥ 4 | > 50 | Y | Y | 15.1 +3.4/-3.6 | 0.34 +0.17/-0.34 | 16.3 +2.0/-2.1 | 0.26 +0.09/-0.10 |
| **CS15** | **≥ 5** | **> 50** | **Y** | **Y** | **15.2 +3.9/-4.4** | **0.32 +0.17/-0.32** | **16.5 +2.6/-2.8** | **0.25 +0.10/-0.14** |
| CS16 | ≥ 5 | > 75 | Y | Y | 14.6 +3.9/-4.3 | 0.30 +0.17/-0.30 | 14.9 +2.4/-2.2 | 0.27 +0.08/-0.12 |

**Table S1.** The different PSVM selection criteria subsets (CS) and their criteria and the Model G fit *a* and *b* parameters for the different applied cut-offs, with their bootstrap uncertainty values. *n* = minimum number of samples per site, *k* is the Fisher precision parameter (Fisher, 1953), 2R and SC give information if the criteria of at least 2 reversals (2R) or correction for serial correlation (SC) have been applied. The subsets in bold are those analyzed in the main manuscript and shown in Figure S1 and S2 of this Supplementary Information file.

**Table S2.** PSVM – $CS7_{vD}$. Locality is the locality number as in Table 1 of the main text. Lat and Long are the average paleolatitude of the locality. N is the number of sites included after the Vandamme cut-off (Vandamme, 1994) was applied. Dec and Inc are the average declination and inclination of the locality. S is the VGP dispersion for that locality with its upper and lower limit. ΔI is the inclination anomaly of that locality with its error. For locality #8, the inclination anomaly is not given as this locality experienced a local block rotation and it's not certain that it has not moved latitudinally. This locality was excluded from any analysis concerning inclination anomaly.

| Locality | Lat (°) | Long (°) | N | Dec (°) | Inc (°) | S (°) | ΔI (°) |
|---|---|---|---|---|---|---|---|
| 1 | 63.3 | 344.1 | 49 | 6.9 | 72.9 | 26.8 +2.9/-3.2 | -3.0 ± 1.9 |
| 2 | 64.1 | 343.9 | 15 | 18.4 | 77.4 | 13.2 +3.6/-4.0 | 1.0 ± 1.5 |
| 6 | 48.0 | 245.3 | 56 | 359.3 | 60.0 | 19.5 +2.5/-2.6 | -5.7 ± 1.7 |
| 8 | 44.5 | 244.1 | 80 | 13.9 | 56.3 | 18.8 +2.1/-2.2 | - |
| 9 | 43.2 | 114.6 | 20 | 355.5 | 57.2 | 9.6 +3.0/-3.5 | -4.8 ± 1.3 |
| 10 | 41.6 | 107.9 | 19 | 12.2 | 60.8 | 14.0 +2.4/-2.6 | 0.2 ± 1.7 |
| 14 | 38.2 | 248.3 | 16 | 351.4 | 51.7 | 24.4 +5.3/-6.0 | -5.9 ± 4.4 |
| 15 | 38.5 | 137.3 | 28 | 6.9 | 50.5 | 21.9 +4.0/-4.3 | -7.3 ± 2.7 |
| 16 | 37.0 | 128.7 | 13 | 2.7 | 55.0 | 26.2 +7.4/-7.6 | -1.4 ± 4.9 |
| 17 | 37.2 | 133.2 | 30 | 8.2 | 47.5 | 20.0 +3.9/-4.2 | -9.1 ± 3.2 |
| 18 | 35.6 | 248.9 | 145 | 354.8 | 48.2 | 16.7 +1.3/-1.3 | -6.8 ± 1.0 |
| 19 | 27.5 | 344.9 | 12 | 352.1 | 41.8 | 12.4 +3.3/-4.0 | -4.4 ± 3.3 |
| 20 | 27.5 | 342.3 | 10 | 0.5 | 38.4 | 15.6 +3.8/-4.6 | -7.7 ± 4.1 |
| 23 | 27.5 | 249.7 | 32 | 352.2 | 43.2 | 17.2 +3.1/-3.2 | -3.0 ± 2.3 |
| 24 | 21.5 | 258.2 | 10 | 0.2 | 35.2 | 16.1 +4.3/-4.5 | -3.0 ± 4.5 |
| 25 | 21.4 | 258.3 | 34 | 351.8 | 29.8 | 9.3 +1.7/-1.8 | -8.3 ± 1.3 |
| 27 | 20.0 | 263.1 | 17 | 344.6 | 36.0 | 21.4 +4.3/-4.6 | 0.0 ± 4.3 |
| 29 | 7.4 | 36.8 | 30 | 0.5 | 8.0 | 14.9 +2.8/-3.0 | -6.6 ± 2.6 |
| 33 | -1.0 | 5.1 | 38 | 358.0 | -6.1 | 11.1 +1.9/-2.0 | -4.0 ± 1.8 |
| 34 | -4.8 | 328.0 | 11 | 358.4 | -17.2 | 15.4 +3.7/-4.2 | -7.5 ± 5.2 |
| 35 | -15.9 | 286.1 | 20 | 353.8 | -33.2 | 16.3 +3.0/-3.3 | -3.6 ± 3.1 |
| 36 | -17.6 | 352.0 | 33 | 356.8 | -20.2 | 21.6 +3.4/-3.6 | 12.1 ± 3.7 |
| 44 | -49.0 | 67.2 | 25 | 5.8 | -61.2 | 22.1 +4.9/-5.5 | 5.4 ± 2.4 |

**Table S3.** PSVM – $CS7_{vD}$ in 10° latitude bins. Bin is the latitude range of the 10° latitude bin. N is the number of sites included after the Vandamme cut-off (Vandamme, 1994) was applied. Dec and Inc are the average declination and inclination of the bin. S is the VGP dispersion for that bin with its upper and lower limit. ΔI is the inclination anomaly of that bin with its error. Locality #8 was excluded from this analysis as it experienced a local block rotation and cannot be combined with other localities from the same latitude bin.

| Bin | N | Dec (°) | Inc (°) | S (°) | ΔI (°) |
|---|---|---|---|---|---|
| -50° – -40° | 28 | 3.2 | -61.3 | 22.0 +4.6/-4.9 | 2.1 ± 2.4 |
| -20° – -10° | 52 | 356.5 | -26.1 | 19.8 +2.5/-2.6 | 2.1 ± 2.5 |
| -10° – 0° | 49 | 358.1 | -8.5 | 12.1 +1.7/-1.8 | 1.4 ± 1.8 |
| 0° – 10° | 36 | 359.6 | 7.5 | 16.7 +3.0/-3.2 | -2.4 ± 2.8 |
| 10° – 20° | 28 | 349.9 | 26.3 | 20.1 +3.7/-3.9 | -1.9 ± 3.5 |
| 20° – 30° | 100 | 354.1 | 36.1 | 13.1 +1.1/-1.2 | -6.9 ± 1.1 |
| 30° – 40° | 225 | 358.1 | 50.1 | 18.9 +1.1/-1.1 | -4.3 ± 0.9 |
| 40° – 50° | 99 | 359.9 | 59.6 | 17.4 +1.7/-1.7 | -3.8 ± 1.0 |
| 60° – 70° | 66 | 8.2 | 75.3 | 24.9 +2.8/-2.9 | -1.6 ± 1.4 |

**Data Set S1.** PSVM.

This file contains all the data in PSVM, with different tabs for different selection criteria. In PSVM Studies, the different localities and studies are presented with their numbers and average Latitude (Lat), Longitude (Long), Paleolatitude (Mlat), Paleolongitude (Mlong), Age in Ma, Number of sites (N), Number of sites after correction for serial correlation (N_SC), whether the locality contains 2 reversals (2R) and whether it is included for the Inclination anomaly analyses (IA). The country of the locality is given in Location, and then the year and authors are presented (same as Table 1 in main text).

In the PSVM_CS1 tab the sites are given separately. 'Site_ID' is the individual number each site has, 'Site' is the name of the site given in the study itself. 'age' is the age in Ma. 'Locality' gives the locality number and 'StudyNr' gives the study number. 'Lat_ave' and 'Long_ave' give the average paleolatitude and paleolongitude for the locality respectively. 'site_lat' and 'Site_Lon' give the precise latitude and longitude of the site, and 'model_lat' and 'model_lon' give the corrected paleolatitude and paleolongitude for that site. 'plate' gives the abbreviation for the tectonic plate on which the site is located. 'dec' and 'inc' give the result for that site in declination and inclination. 'Ndir' gives the number of samples used for that result. 'kdir' gives the k value from that result. 'alpha95' gives the $\alpha_{95}$ value for that result. 'Polarity' gives N for normal polarity, R for Reverse polarity and T for Transitional polarity. 'Dec_norm' and 'Inc_norm' give the declination and inclination for that result after being normalized to normal polarity. 'Model_vgp_lat' and 'model_vgp_lon' give the latitude and longitude for the virtual geomagnetic pole calculated from the directional result and paleolatitude and paleolongitude from that site. 'location' and 'PSVM_location' give the country and more specific location of the locality and 'reference' gives the first author and year of publication.

The other tabs have the same headings, and represent the different subsets (CS2 – CS16) for the different selection criteria. The final two tabs are of CS1 but with only normal or reversed data, respectively.